ACS NANO

www.acsnano.org

ARTICLE

Highly Branched Au Superparticles as Efficient Photothermal Transducers for Optical Neuromodulation

Xinyu Cheng,[‖] Wenjun Li,[‖] Yinghan Wang,[‖] Kangkang Weng,[*] Yunyun Xing, Yunxiang Huang, Xing Sheng, Jun Yao,[*] Hao Zhang,[*] and Jinghong Li[*]

Cite This: *ACS Nano* 2024, 18, 29572−29584

Read Online

ACCESS | Metrics & More | Article Recommendations | Supporting Information

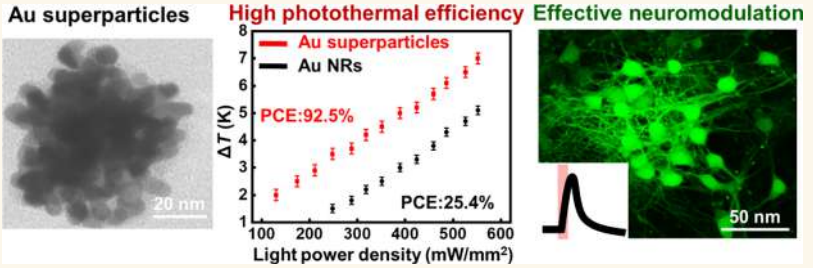

ABSTRACT: **Precise neuromodulation is critical for interrogating cellular communication and treating neurological diseases. Nanoscale transducers have emerged as effective interfaces to exert photothermal effects and modulate neural activities with a high spatiotemporal resolution. Ideal materials for this application should possess strong light absorption, high photothermal conversion efficiency, and great biocompatibility for clinical translation. Here, we show that the structurally designed 3D Au superparticles with a highly branched morphology can be promising candidates for nongenetic and remote neuromodulation. The structure-induced blackbody-like absorption endows Au superparticles with photothermal conversion efficiency over 90%, much higher than that of conventional Au nanorods. With the biocompatible polydopamine ligands, Au superparticles can be readily interfaced with primary mouse hippocampal neurons and other cells and can photostimulate or inhibit their activities in both cell networks or with a single-cell resolution. These findings highlight the importance of structural designs as powerful tools to promote the performance of plasmonic materials in neuromodulation and related research of neuroscience and neuroengineering.**

KEYWORDS: *Au superparticles, structural designs, photothermal effect, neural interfaces, neuromodulation*

INTRODUCTION

The capabilities of modulating neural activities are important for studying the complex neuronal functions and treating neurological diseases.[1,2] As widely used tools for neuromodulation, traditional electrical implants can stimulate or inhibit neural activity with high precision. However, this approach typically suffers from the bulky and wired configuration, mechanical invasiveness, and the associated inflammatory responses and tissue damage.[3−5] Alternatively, optogenetics and related techniques enable light-triggered, remote, and wireless neuromodulation with an ultrahigh spatiotemporal resolution and cellular specificity.[2,6,7] However, optogenetics relies on the transfection of light-sensitive ion channels in cell membranes. Such a need of genetic modification impedes its immediate clinical translation.[8,9]

More recently, optically active functional materials have been leveraged in the nongenetic version of light-triggered, remote neuromodulation.[10−13] This strategy requires no bulky device implantation or genetic modification. It also promises minimally invasive neuronal regulation with a high spatiotemporal resolution inherent from optical stimulation.[10] The key to this strategy lies in the designs of functional materials.[3,11,14,15] Various inorganic[16,17] and organic[18−20] conductors and semiconductors,[21,22] in their conventional or nanoscale

Received: May 30, 2024
Revised: October 3, 2024
Accepted: October 8, 2024
Published: October 14, 2024

https://doi.org/10.1021/acsnano.4c07163
ACS Nano 2024, 18, 29572−29584

forms, can be interfaced with unmodified neurons, tissues, or organs. Under illumination or other stimuli, these materials produce physical or chemical stimuli via photothermal,[8,17,23,24] photocapacitive,[16,18,19,21,22,25−29] photofaradaic,[12,16,30−32] and other pathways.[33,34] These stimuli can then induce the depolarization or hyperpolarization of neurons and even regulate the behaviors of animal models.[16]

Nanoscale photothermal transducers are representative materials for nongenetic neuromodulation.[35] For example, plasmonic 0D Au nanoparticles and 1D Au nanorods (NRs) have been widely used to convert optical energy into heat (or temperature changes), with broad applications in sensing, therapy, and imaging.[36,37] More recently, these Au-based model systems also show great potential in the photothermal stimulation or inhibition of neural activities under laser illumination.[8,38] In brief, intense illumination at the Au nanomaterial−neuron interface introduces rapid temperature increases and transient changes in neuron membrane capacitance. This optocapacitive process induces membrane depolarization and subsequent neuron excitation.[8,39] Conversely, mild illumination can also cause relatively slow temperature increases, which can inhibit neural activity via some endogenous and thermosensitive potassium ion channels.[38,40−42] Importantly, the modulation can be performed with a micrometer-scale spatial and millisecond-scale temporal resolution, offering valuable insights into studies from single neuron firing to rhythmic patterns in neuron networks.[42]

Despite the progress achieved with these conventional types of Au nanomaterials, rational designs of photothermal transducers can further advance photothermal modulation in both fundamental studies and clinical applications. Ideally, the photothermal transducers should possess (1) high absorption efficiency, especially in the near-infrared regime, for applications in deep tissues of *in vivo* animal models; (2) high photothermal conversion efficiency for minimizing the illumination energy and avoiding irreversible cell dysfunction or tissue damage; (3) great biocompatibility for integrating with neurons and tissues at their interfaces; (4) versatility in the synthesis and diverse material designs for targeted neuron types and physiological studies. For example, the frequently used 1D plasmonic Au NRs show a large light scattering cross section and direction- and polarization-dependent absorption, which limit their photothermal conversion efficiency to below 50% under polarized laser illumination. Materials with enhanced photothermal conversion efficiency are favored. One promising approach is to use nanomaterials with other compositions, including those based on carbon,[43−45] silicon,[16,17,30,46] and transition metal carbides (MXenes).[47] Alternatively, structural or morphological control, a well-established strategy for promoting the performance of nanomaterials in photothermal therapy and photoacoustic imaging, would offer more freedom in the search for ideal candidates for neuromodulation. However, despite some examples using structured silicon[17] or antibody-mediated clustered Au nanoparticles,[8] this strategy has been much less employed in photothermal neuromodulation[17,41,47,48] compared to the case of photothermal therapy.

Here, we show that the structural engineering of plasmonic transducers can be a powerful approach to enhance the efficiency of photothermal neuromodulation. We synthesize 3D Au superparticles with highly branched structures following protocols reported by Yin and co-workers.[48] The 3D structures endow Au superparticles with broadband and blackbody-like absorption covering the entire visible and near-infrared spectrum. The term "blackbody-like absorption" refers to the feature that light of all wavelengths and angles can be nearly perfectly absorbed by the material to show the flat, broadband absorption. Some examples of plasmonic blackbody-like absorbers have been reported in recent work.[48−50] Specifically, the small scattering cross section and direction-independent absorption of Au superparticles lead to exceptionally high photothermal conversion efficiency (>90%), which compares favorably over traditional Au NRs (<50%). The polydopamine ligands used in synthesizing Au superparticles also render them fully biocompatible when interfacing with primary mouse hippocampal neurons and other cells. Under different illumination intensities with a near-infrared laser (∼800 nm), Au superparticles can produce heat with higher efficiency (namely, achieve the same temperature increases at lower light intensities) than the Au NRs and can modulate the activities of the neural networks or a single cell. These results show the great potential of 3D branched Au superparticles in nongenetically modulating neural activities and also highlight the importance of structural engineering, a well-established methodology in nanoscience, neuromodulation, and related studies.

RESULTS AND DISCUSSION

Morphology and Broadband Absorption of Highly Branched Au Superparticles. The highly branched Au superparticles were synthesized following reported protocols (Figure 1a).[48] In brief, Au nanoparticles (average diameter, ∼14 nm) coated with polyvinylpyrrolidone (PVP) ligands were used as seeds for the subsequent growth of Au via the reduction of $HAuCl_4$ in a Tris-HCl buffer solution. The key to the growth of branched superparticles is the use of polydopamine ligands, which constantly modulate the chemical potential of the growing surface and enable continuous deposition of Au islands in the Volmer−Weber mode. The Volmer−Weber mode corresponds to the situation that the growing Au tends to self-nucleate to form islands and branches on the preformed Au cores/nuclei instead of undergoing layer-by-layer growth to form a regular shell on the cores due to the increased chemical potential during growth. The cores and branches are firmly bonded via their interfaces in the superparticles with voids between the branches (Figure 1b and Figure S1), which makes the superparticles different from the assembly of isolated Au nanoparticles. The presence and contents of polydopamine ligands can be validated by energy-dispersive X-ray spectroscopy (EDS), Fourier transform infrared (FTIR) spectroscopy, and thermogravimetric analysis (TGA), as shown in Figure S1. The mass ratio of polydopamine ligands in the superparticles is about 12%, which translates to an ∼32.3% volume ratio of solid Au in the superparticles in the total volume of Au and polydopamine ligands. These polydopamine ligands also endow Au superparticles with great biocompatibility, as discussed later. The obtained Au superparticles after 6 h of reaction show a multibranched geometry and an average size of ∼60 nm (Figure 1b). They can form dispersions in water and phosphate-buffered solution (PBS, 0.01 M) with good colloidal stability. Note that some aggregates form in the solution after several hours, which can redisperse in the solvents after a brief vortex or sonication. Modifying the ligands may improve the long-term colloidal stability of the superparticles. The black color of Au superparticles is distinct from the color of

https://doi.org/10.1021/acsnano.4c07163
ACS Nano 2024, 18, 29572−29584

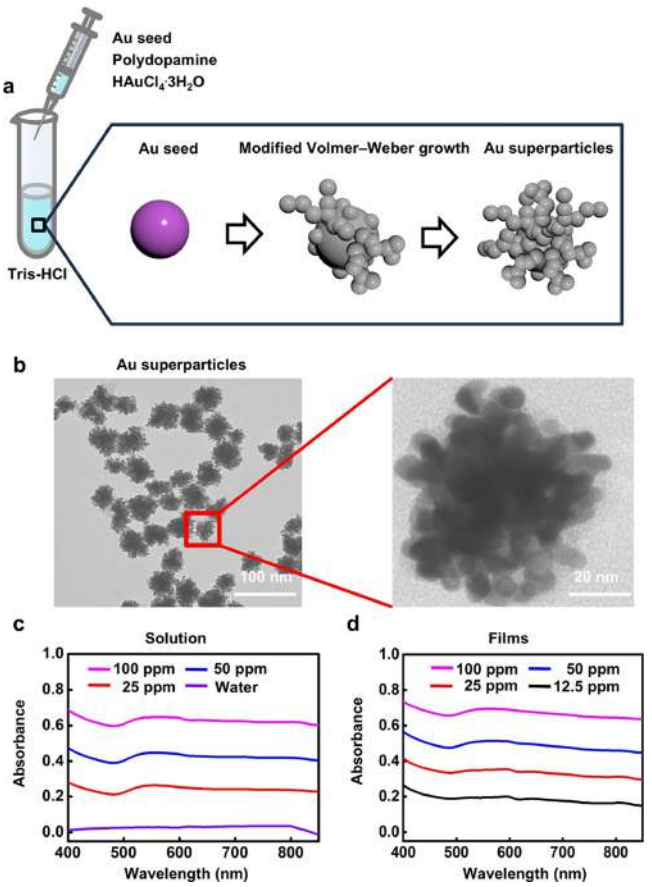

Figure 1. Synthesis and broadband absorption of highly branched Au superparticles. (a) Schematic illustration of the synthesis for highly branched Au superparticles. (b) TEM images of Au superparticles. (c,d) Optical absorption spectra of (c) Au superparticle solutions of different concentrations and (d) films spin-coated from these solutions.

conventional 0D Au nanoparticles or 1D NRs used for neuromodulation.[8,38,44,51] Optical spectra of Au superparticle dispersions of different concentrations and corresponding coated films (Figure 1c,d) reveal strong, broadband, and blackbody-like absorption features. Even with a low concentration of 25 ppm, the Au superparticle dispersion shows notable absorption covering the entire visible and near-infrared regions. Such optical features stem from a combination of substantial plasmonic coupling and effective light trapping effects in the branched superparticles.[48] The latter decreases the scattering cross section (σ_{sca}) and leads to the improved light absorption efficiency (defined as $\sigma_{abs}/(\sigma_{abs} + \sigma_{sca})$, σ_{abs}, the absorption cross section) of over 95%, as estimated in previous reports.[48,52,53] The broadband absorption can be attributed to the superposition of multiple or high-order scattering events from the multiple hot spots in the 3D superparticles.[48,49]

Photothermal Conversion Efficiency of Au Superparticles. The blackbody-like absorption of Au superparticles translates into high photothermal conversion efficiency, which can be calculated from measured data by using Roper's method.[54,55] In detail, we monitored the temperature increases of Au superparticle dispersions (100 ppm, O.D. ~ 0.7) with an infrared thermal imaging camera during continuous laser irradiation (808 nm, 10 mW/cm^2). The choice of 808 nm is because illumination of this wavelength is typically used for studying the efficacy of Au NRs and other nanomaterials in photothermal neuromodulation due to its high tissue penetration depth.[38,42,47,56,57] As shown in Figure 2a and

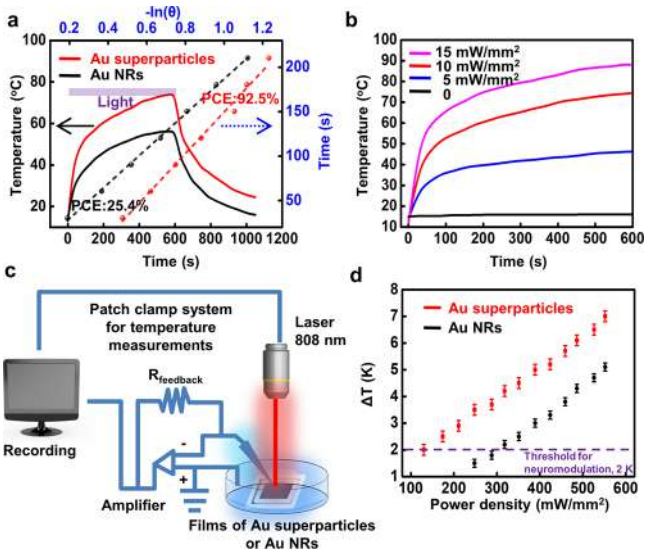

Figure 2. Characterizations of photothermal properties of Au superparticles. (a) Temporal temperature changes (solid lines) of aqueous solutions of Au superparticles and NRs (100 ppm) under 808 nm irradiation (10 mW/cm^2). The purple bar indicates the irradiation duration. The dashed lines are the derived time constants (τ_s) for heat transfer (see experimental methods), which allow for calculating the photothermal conversion efficiency (PCE) of the corresponding samples. (b) Temporal temperature changes of a Au superparticle solution (100 ppm) under 808 nm irradiation at various laser power densities. (c) Schematic diagram of the patch clamp system for measuring instantaneous (1 ms) temperature changes near the films of Au superparticles or NRs induced by laser irradiation. (d) Maximum temperature changes for films of Au superparticles and NRs under 808 nm laser irradiation (1 ms) as a function of laser power densities.

Figure S2, the temperature of Au superparticle solution increases from ~15 to ~75 °C during the period of laser irradiation (10 min) and decreases to ~20 °C via natural cooling after stopping irradiation. Based on the maximum and environmental temperature as well as other parameters[54] (e.g., the time constant for heat transfer shown as the *y*-axis on the right of Figure 2a, Experimental Section), the photothermal conversion efficiency of Au superparticles was calculated to be 92.5%. This value is consistent with that in a previous report.[48] For reference, we also monitored the temperature changes of Au NR dispersions (the aspect ratio of Au NRs is about 3.5) under the same condition. The photothermal conversion efficiency of Au NRs was estimated to be ~25.4%, similar to reported values.[58,59] Note that the concentrations of Au atoms/element in the 100 ppm solution of Au superparticles and NRs were 88 and 77 ppm, respectively, according to the TGA data. This suggests that with similar concentrations of Au atoms or elements, Au superparticles show much higher photothermal conversion efficiency and temperature increases under similar illumination conditions. Therefore, the enhanced photothermal conversion efficiency in superparticles is from the structural designs instead of changes in the number of Au atoms. Although the superparticles show a lower absorption coefficient than the NRs at 808 nm (Figure S 2d), the highly branched geometry of the former may confine most of the

https://doi.org/10.1021/acsnano.4c07163
ACS Nano 2024, 18, 29572−29584

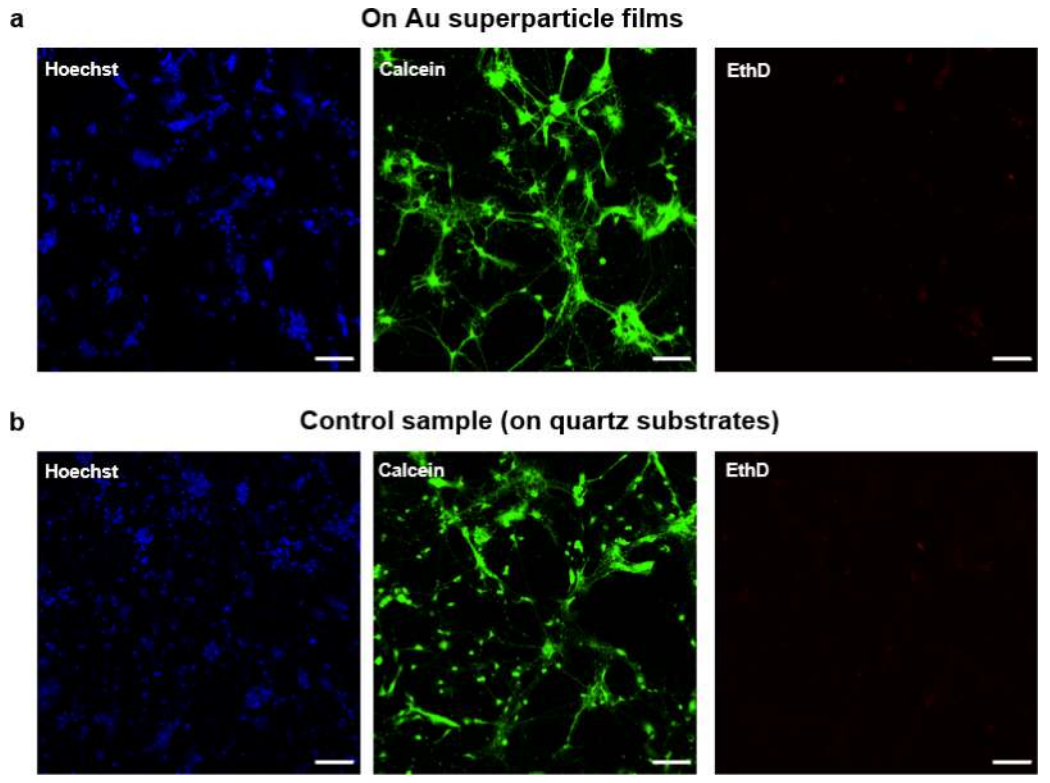

Figure 3. Cell biocompatibility of mouse hippocampal neurons cultured on Au superparticle films. (a) Live/dead assay of mouse hippocampal neurons incubated on Au superparticle films and (b) bare quartz substrates for 7 days. The images with blue (Hoechst), green (Calcein AM), and red (ethidium homodimer-1, EthD) colors represent cell nuclei, live cells, and dead cells, respectively. Scale bars are 100 μm.

incident light within the structures, which can strongly reduce σ_{sca} and increase the photothermal conversion efficiency. Similar contrast in the absorbance and photothermal conversion efficiency was also observed in a previous report.[48] Additionally, the measured temperature changes increase with both the concentration of Au superparticles and the laser power density, as shown in Figure 2b and Figure S2. With a relatively low irradiation power density (~5 mW/mm^2), the temperature of the Au superparticle dispersion can increase by ~25 °C (Figure 2b). For reference, other efficient Au-based photothermal transducers, such as Au nanostars (O.D. ~ 0.7),[60] cause smaller temperature increases (<15 °C) under similar illumination conditions.

Complementary to the photothermal conversion efficiency estimated from solution samples, the measurements of film samples can better represent the neuromodulation process at the material/neuron interface. The measurements for Au superparticle films used a calibrated micropipette resistance method[16,47] that provided transient temperature changes near the film, as schemed in Figure 2c. The films were coated from 100 ppm solutions to achieve relatively high density and film quality (Figure S3). These films also show high reproducibility in photothermal and *in vitro* tests. We thus used 100 ppm solution to make films for the following experiments. Illuminating the Au superparticle films (with superparticles obtained after the reaction of 6 h) with a near-infrared laser (808 nm, 1 ms pulse, ~4 mm spot size, and a film size of 1 cm × 1 cm) leads to transient temperature changes, which range from 2 to 7 K by varying the incident laser power density from 130 to 550 mW/mm^2 (Figure 2d and Figure S4). The 1 ms illumination period resembles that used in neurostimulation and thus provides guidance in the efficacy of nanotransducer films in modulating neuronal activities. Note that the typical temperature increase required for neuromodulation without heat damage is about 1−3 K. We thus set the threshold temperature increases for neuromodulation as 2 K (the dashed line in Figure 2d). To achieve the same temperature changes after 1 ms of irradiation, Au superparticles need less than half of the laser power required for Au NRs (Figure 2d), highlighting their great potential in neuromodulation. We also evaluated the temperature increases induced solely by the polydopamine films (Figure S5). No temperature increases were detected for irradiated polydopamine films below 300 mW/mm^2. This result excludes the contribution of polydopamine ligands to the heat generation in Au superparticles. We can make a rough comparison in the photothermal conversion efficiency of Au superparticles and other recently reported nanoscale photothermal transducers for neuromodulation (Table S1). Under similar irradiation conditions, the temperature increases for solutions containing Au superparticles are higher than those of other nanotranducers. We also compared the morphologies and photothermal conversion efficacy of Au superparticles obtained with different reaction times (Figure S6). Samples obtained after the reaction for 3 h show an average diameter of ~20 nm and a limited number of branches. Samples synthesized for 8 or 12 h show a similar degree of structural branching or complexity with those synthesized for 6 h but much lower colloidal stability (Figure S7). The temperature increases for superparticles synthesized for 6, 8, and 12 h are also comparable (Figure S6f) and higher than those for samples synthesized for 3 h. Therefore, we used

https://doi.org/10.1021/acsnano.4c07163
ACS Nano 2024, 18, 29572−29584

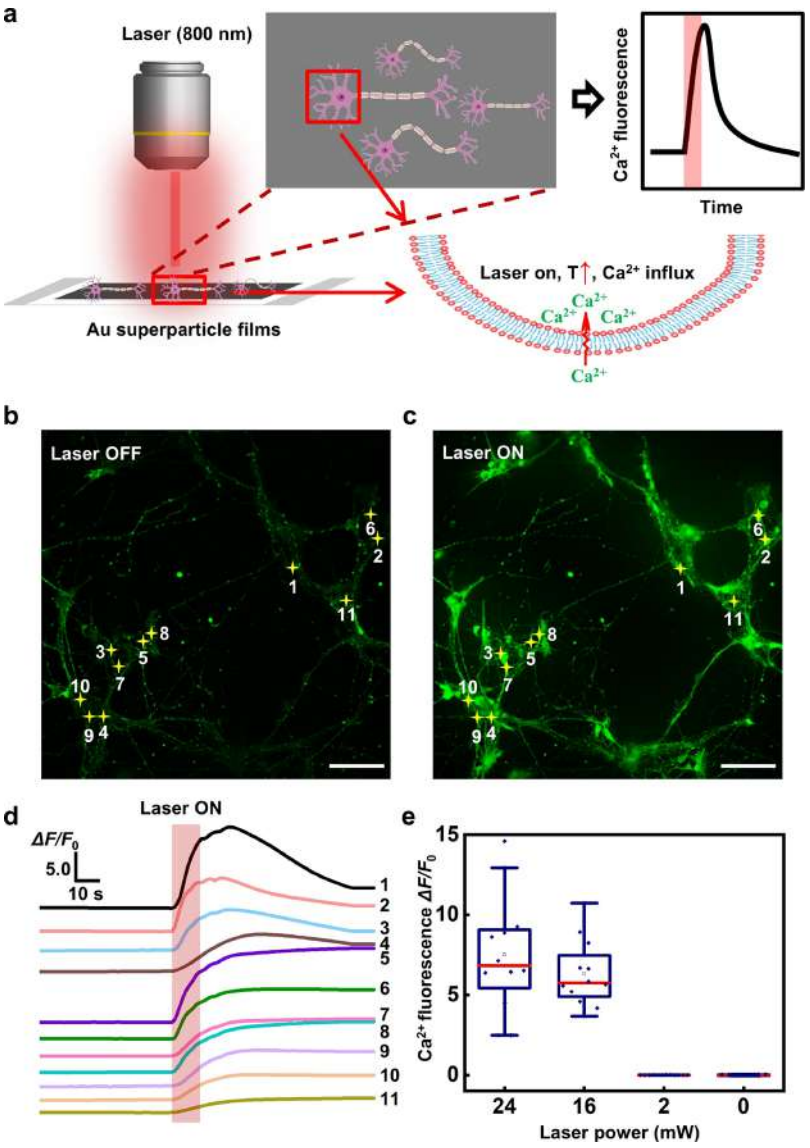

Figure 4. Photothermal stimulation of mouse hippocampal neurons cultured on Au superparticle films. (a) Scheme for the laser stimulation of mouse hippocampal neurons cultured on Au superparticle films and calcium imaging with a confocal microscope. The photothermal effect increases the temperature near the cell membrane and incurs Ca^{2+} influx. (b,c) Sample images of calcium imaging of stained hippocampal neurons (Ca^{2+} indicator, Calbryte 520 AM) cultured on Au superparticle films taken when the 800 nm laser is (b) off and (c) on. The laser power was 24 mW. The 11 neurons marked with yellow crosses were selected randomly as ROIs for fluorescence analysis. Scale bars are 100 μm. (d) Normalized calcium fluorescence intensity changes ($\Delta F/F_0$) of the ROIs of the 11 selected neurons as a function of time. The red bar indicates the laser illumination time (10 s). (e) Distribution of the normalized $\Delta F/F_0$ of neurons at different laser powers (24, 16, 2, and 0 mW). The statistics were based on data from all ROIs of the marked neurons.

superparticles synthesized for 6 h for the following experiments.

Biocompatibility of Au Superparticles. It is important to note that although widely considered biocompatible and used in various biomedical applications, Au nanomaterials with some types of geometries and surface chemistries can be detrimental to cell viability. For instance, cetyltrimethylammonium bromide (CTAB), commonly adopted as the ligand for the synthesis of Au nanoparticles and NRs, has been reported to be toxic to neurons.[61,62] It is thus important to ensure the biocompatibility of the branched Au superparticles. Figure 3 shows the fluorescence images of primary hippocampal neurons cultured for 7 days and stained using a LIVE/DEAD cell imaging kit. Neurons cultured on both Au superparticle films and bare quartz plates showed a good cellular morphology and density without noticeable cell toxicity. We also assessed the viability of cultured Michigan Cancer Foundation-7 (MCF7) cells (Figure S8) using a CCK-8 assay. The estimated cell viabilities are almost 100%. The good biocompatibility of Au superparticles is related to polydopamine ligands. Additional polydopamine coating on Au nanomaterials has been reported to minimize cytotoxicity and enhance the adhesion between Au and neurons.[41] In our case, the native polydopamine ligands of as-synthesized Au superparticles obviate the requirements for postsynthetic surface modification or additional coating steps.

Photothermal Modulation of Neural Activities. Previous reports[44,51,60,63] have demonstrated that the photothermal effects from Au NRs and other transducers can either stimulate or suppress the neuronal activities, depending on the

https://doi.org/10.1021/acsnano.4c07163
ACS Nano 2024, 18, 29572−29584

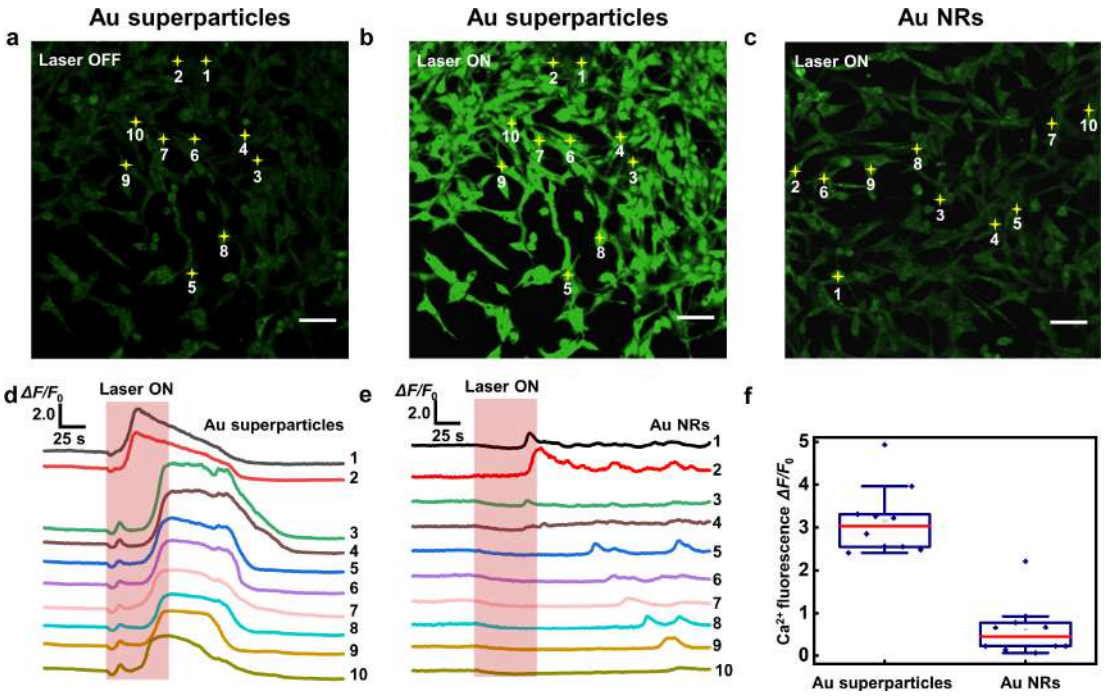

Figure 5. Comparison of films of Au superparticles and NRs in cell activity stimulation. (a,b) Calcium imaging of PC-12 cells (stained with the Ca^{2+} indicator, Calbryte 520 AM) cultured on Au superparticle films when the laser (808 nm, 55.2 mW/mm^2) is (a) off and (b) on. The cells marked with yellow crosses indicate ROIs selected randomly for fluorescence analysis. (c) Calcium imaging of PC-12 cells (stained with the Ca^{2+} indicator, Calbryte 520 AM) cultured on Au NR substrates when the laser is on. The stimulation and imaging conditions were identical for samples in (b). (d,e) Normalized $\Delta F/F_0$ of PC-12 cells marked in (b,c) cultured on (d) Au superparticle and (e) Au NR films. The red bars indicate the laser illumination time (1 min). (f) Comparison of normalized $\Delta F/F_0$ for photostimulated PC-12 cells cultured on Au superparticle and Au NR films. The statistics were based on data from all of the ROIs of the marked cells. Scale bars are 100 μm.

illumination condition, the dynamics of temperature changes, and the involved ion channels in the cell membrane. The branched Au superparticles can also achieve bidirectional modulation of neuronal activity for the neural network or a single neuron but with much higher efficiency than conventionally used Au NRs.

We first tested the capabilities of Au superparticles in stimulating the network of primary mouse hippocampal neurons. For this experiment, neurons cultured on Au superparticle films were loaded with Calbryte 520 AM indicators, and their activities were monitored using Ca^{2+} imaging. Because Ca^{2+} channels can be synchronously activated by action potential firing, the events of intracellular Ca^{2+} fluorescence changes can be used to depict the activity of the neurons and neural networks.[64,65] The confocal microscope for fluorescence imaging was equipped with an 800 nm laser for photothermal conversion and a 488 nm laser for exciting the fluorescent Ca^{2+} indicators (Figure 4a). The wavelength of the equipped laser (800 nm) is slightly different from the external laser (808 nm) used for testing the photothermal conversion efficiency, but the absorption features of Au superparticles (or Au NRs) at these two wavelengths are almost identical. Note that in these experiments, the entire field of view was illuminated by the 800 nm laser and imaged, which provided the information on all neurons in the field. Prior to turning on the 800 nm laser, the images were taken for ~50 s to record the baseline for Ca^{2+} fluorescence intensities of the neurons (as indicated by the yellow crosses in Figure 4b,c, where the ROIs were areas covering the nearby cell). Illuminating with the 800 nm laser (12% of the full power, or ~24 mW) for 10 s results in rapid increases in the Ca^{2+} fluorescence ($\Delta F/F_0$) by more than 5 times (or >500%) (Figure 4d,e is based on data collected from neurons marked by the yellow crosses). The maximum $\Delta F/F_0$ can reach ~14.6-fold. Ceasing the illumination results in a gradual decrease in the Ca^{2+} fluorescence and neural network activity. Such substantial changes in Ca^{2+} fluorescence corroborate the high photothermal conversion efficiency of Au superparticles. The magnitude of fluorescence changes can be tuned by adjusting the illumination intensity (Figure S9). Reducing the relative power density of the 800 nm laser from 12 to 8% (or ~24 to 16 mW) slightly decreases the averaged $\Delta F/F_0$ from ~7.5 to ~6-fold. Decreasing the relative light power density to 1% (2 mW) leads to negligible Ca^{2+} signaling in the hippocampal neurons, probably due to insufficient transient temperature changes. In parallel, we also monitored the expression of c-Fos, which is an immediate early gene that can rapidly express in response to the influx of Ca^{2+} ions and thus can serve as an indicator of neuronal activity.[66] The upregulation of c-Fos, as shown in the immunohistochemical images (Figure S10), corroborates the photothermal activation of neural activities. Additionally, we checked the possibility of cell damage after photostimulation. Mouse hippocampal neurons cultured on Au superparticle films remain alive after stimulation by an 808 nm laser (intensity, 55.2 mW/mm^2 and a duration of 10 s), as shown in Figure S11. A previous report suggests that the threshold temperature for local neuron damage is about 60 °C.[67] This suggests that the local temperature increases during neuromodulation in our case are still in the safe regime and insufficient to cause neuronal damage. We also performed control experiments on neurons cultured on polydopamine films, which show no changes in the intensity of Ca^{2+}

https://doi.org/10.1021/acsnano.4c07163
ACS Nano 2024, 18, 29572−29584

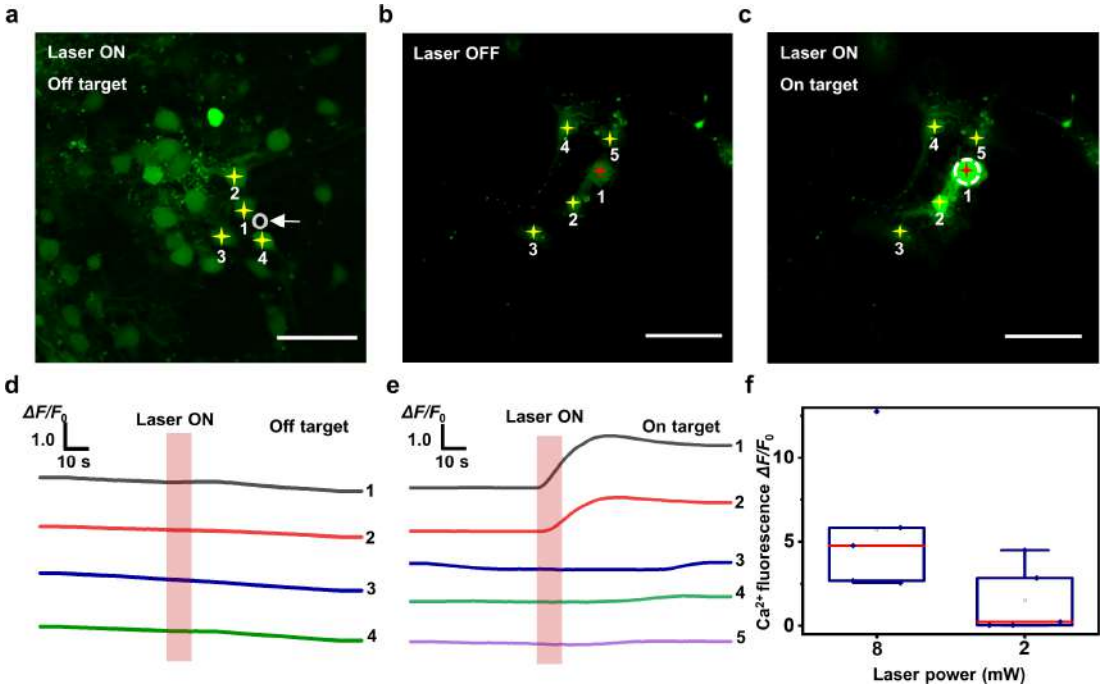

Figure 6. Modulation of target neurons cultured on Au superparticle films. (a) Sample images of calcium imaging of mouse hippocampal neurons (stained with the Ca^{2+} indicator, Calbryte 520 AM) cultured on Au superparticle films. The white circle indicates the focus of the stimulation laser. As the focus is in the off-cell area, neurons (#1−4) show low Ca^{2+} fluorescence changes even at a laser power of 24 mW. (b,c) Calcium imaging of mouse hippocampal neurons cultured on Au superparticle films when the laser is (b) off and (c) on. In (c), the laser was focused on target neuron #1 (indicated by the white dashed circle), which increases the Ca^{2+} fluorescence of this neuron, even at a low laser power (2 mW). (d,e) Normalized $\Delta F/F_0$ over time of neurons marked in (a) and (c), respectively. The red bars denote the laser illumination time (24 and 2 mW, respectively, 10 s). In addition to the fluorescence of the ROI of the target neuron (#1), ROIs of other neurons indicated by the yellow crosses in panels (a) and (c) are also used for fluorescence analysis. (f) Comparison of normalized $\Delta F/F_0$ for neurons irradiated at different laser powers. The statistics were based on data from all ROIs of the marked cells. Scale bars are 50 μm.

fluorescence under identical illumination/stimulation conditions (Figure S12).

We then compared the efficacy of Au superparticles and Au NRs in modulating cell activities. To this end, we used PC-12, a widely accepted neuronal line model.[68] Under identical illumination and Ca^{2+} imaging conditions, PC-12 cells cultured on Au superparticle films show on average of ~3-fold increases in $\Delta F/F_0$, whereas those on Au NR films exhibit much smaller and slower changes ($\Delta F/F_0 < 1$, Figure 5 and Figure S13). The contrast is consistent with the differences in the Au superparticles and NRs in the photothermal conversion efficiency. Au superparticles can also be used to modulate the activity of other types of cells, such as the breast cancer MCF7 cells (Figure S14).

In addition to wide-field illumination and stimulation, focusing the light to a much smaller area can selectively activate a single target neuron. Such a focal stimulation method can accompany a high spatiotemporal resolution, which is critical for interrogating complex neuronal functions, including electrical/chemical communication between neurons and their synchrony.[42,47,57,69] As a proof of concept, we selectively targeted a single or a limited number of primary hippocampal neurons (focus spot size, ~400 μm^2) and monitored the dynamic Ca^{2+} fluorescence changes of the target and neighboring neurons. As a control experiment, we first focused the laser to an off-cell area (marked by the white circle in Figure 6a), which was at least 5 μm away from neurons #1−4 (Figure S15). Even at a high power density (24 mW, 10 s illumination), the off-target illumination introduces no detectable changes in the fluorescence intensities (Figure 6d). By contrast, focusing light on target neurons can successfully upregulate Ca^{2+} fluorescence of the target neuron with a much lower power (2 mW). As shown in Figure 6b,c, the target neuron (no. 1, marked by the red cross) shows a large $\Delta F/F_0$ of ~4.5, while the neighboring neurons (cells #3−5, marked by the yellow crosses) exhibit minimal changes in fluorescence (Figure 6e). However, it is interesting to note that neuron #2, which is also in the nonstimulated region, shows a rapid increase in $\Delta F/F_0$ with a similar magnitude.[57] As neurons #2 and #5 are similarly distant from #1 but show drastically different responses, we tend to ascribe the activation of neuron #2 to intercellular communication via synaptic connection.[69]

We also found that the activity of the neural network after the stimulation of a single cell can be strongly affected by the illumination power. By elevating the relative laser power to 8 mW (or 4% of the full power of the laser, Figure 6f and Figure S16), the target neuron #1 and its neighbors (#2−5) are activated, which is different from the above case with a lower stimulation power. The activation of neighboring neurons may be due to the larger temperature increases at an elevated stimulation power, which may lead to the synchrony of neuronal activity via the action potential propagation within the neural network.[69,70] It is also interesting to note that the neighboring neurons were activated at different times. Neurons #2 and #3 were activated at almost the same time with target neuron #1, while there was a notable lag for activating neurons #4 and #5. We also used MCF7 cells cultured on Au superparticle films as control samples (Figure S17). MCF7 cells have no synaptic connections or neurotransmitter propagation. We illuminated a single MCF7 cell (no. 1) with

https://doi.org/10.1021/acsnano.4c07163
ACS Nano 2024, 18, 29572−29584

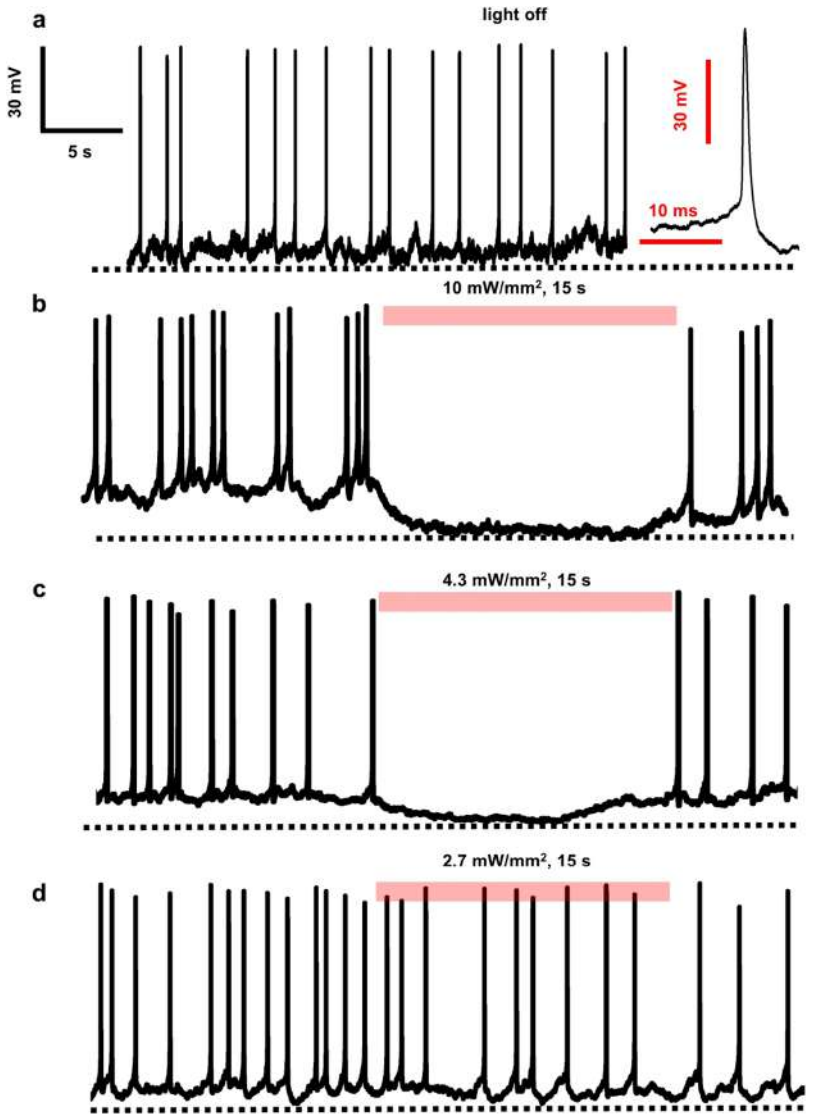

Figure 7. Inhibition of neuronal activity under continuous irradiation. (a) In the absence of light, the mouse hippocampal neuron cultured on Au superparticle films can be excited with positive current injection via a micropipette. The right panel is the data of a single neuron, whose timescale is indicated by a red line (10 ms). The timescale for the recorded membrane potentials before and after illumination is indicated by the black horizontal axis on the top-left corner. (b,c) Under continuous 808 nm laser irradiation (15 s, 10 and 4.3 mW/mm^2 for (b) and (c)), the action potential firing was inhibited. The red line indicates the laser irradiation time. (d) At a lower laser power density (2.7 mW/mm^2), the action potential firing was not effectively inhibited. Number of neurons = 3.

a higher light power (24 mW), which was expected to introduce larger temperature increases near MCF7 cell no. 1. However, rather than synchronicity, there is a notable delay in the excitation for target and neighbor cells. The delayed excitation suggests a different intercellular communication pathway, probably the Ca^{2+} propagation via gap junctions or responses to ATPs released from the stimulated cells.[69] Note that the origin of observations related to the single-cell stimulation experiments can be very complex and needs more in-depth and systematic investigation. Nonetheless, the contrast in the performance of stimulated mouse hippocampal neurons and MCF7 cells suggests that Au superparticles can be used as a photothermal platform for understanding the correlation and circuitry of neural networks, especially when integrated with recording tools.

Contrary to the photostimulation effect triggered by intense light, low-power illumination can inhibit neuronal activity, as demonstrated by a series of work with Au NRs.[23,38] Similarly, Au superparticle films can also fully suppress neuronal activities by inducing hyperpolarization, and the membrane potential is more negative. In detail, mouse hippocampal neurons were cultured on Au superparticle films, and the membrane potential was recorded by a whole-cell patch clamp recording system. We electrically activate neurons by injecting positive currents until they elicit action potentials (or spikes), as shown in Figure 7a. After continuous 808 nm illumination for 15 s (10 or 4.3 mW/mm^2), the action potential of neurons cultured on Au superparticle films (number of neurons = 3) disappears within about 1−5 s (Figure 7b,c and Figures S18 and S19). The signals recover after ceasing the illumination. The illumination power density required for Au superparticles to fully suppress the action potentials of mouse primary hippocampal neurons is comparable or slightly lower than that needed for Au NRs (~15−50 mW/mm^2).[23] When the power density decreases to 2.7 mW/mm^2, the decline in the action potentials can be neglected (Figure 7d). We also

https://doi.org/10.1021/acsnano.4c07163
ACS Nano 2024, 18, 29572−29584

performed control experiments with neurons cultured on bare quartz substrates (number of neurons = 3, Figures S20 and S21). Without Au superparticles, illumination with a power density of 10 mW/mm^2 cannot suppress neuronal activities.

CONCLUSIONS

In conclusion, we show that highly branched Au superparticles can serve as efficient transducers for nongenetic photothermal neuromodulation. The broadband and blackbody-like absorption endow the Au superparticles with ultrahigh photothermal conversion efficiency (>90% versus <50% for Au NRs), while their native polydopamine ligands provide great biocompatibility. The combined features allow Au superparticles to increase the temperature near the neuron interface and modulate neuronal activities with much lower laser energies than that required for conventional Au nanomaterials. The capabilities of effective and bidirectional stimulation/inhibition with a single-cell resolution under near-infrared illumination promise the use of Au superparticles in studying the complex circuitry of neural networks. Moreover, films of Au superparticles may also function as implantable devices to wrap around nerves or form conformal contact with the brain cortex, similar to other film devices in previous reports,[16,18,26,71] for photothermal modulation of peripheral and central nervous systems. We expect that the rational structural design of Au and other photothermal nanomaterials, benefiting from the advances in nanomaterials synthesis during the past decades, can boost the progress in finding suitable material platforms for understanding neural communication, controlling engineered tissues, and treating neurological disorders.

EXPERIMENTAL SECTION

Synthesis of 3D Branched Au Superparticles. The synthesis followed previously reported protocols.[48] First, Au nanoparticles with an average diameter of 14 nm were synthesized by seeded growth. In step 1, small Au seeds were prepared by mixing 0.5 mL of $HAuCl_4$ solution (5 mM) and 0.5 mL of trisodium citrate solution (5 mM) in 9 mL of deionized water followed by the quick injection of an aqueous solution of $NaBH_4$ (0.3 mL, 0.1 M) under vigorous stirring. The solution immediately turned yellowish red in color. The solution was stirred for 4 h before being stored at 4 °C for subsequent seed growth. In step 2, solutions of potassium iodide (1 mL, 0.2 M), polyvinylpyrrolidone (2.5 mL, 5 wt %), $HAuCl_4$ (1.25 mL, 25.4 mM), and ascorbic acid (1.25 mL, 0.1 M) were mixed with 7.3 mL of deionized water. Three mL of the Au seed solution (prepared in step 1) was quickly injected into this solution under vigorous stirring. After 10 min, the product (Au nanoparticles with an average size of about 14 nm) was collected by centrifugation and redispersed in 52 mL of deionized water.

The Au nanoparticles were then used as seeds for the growth of 3D highly branched superparticles. Under a nitrogen flow, 100 μL of Au nanoparticle solution was added to 9 mL of a Tris-HCl buffer (pH = 8.5). Then, dopamine (50 μL, 4 mg/mL) and $HAuCl_4$ (100 μL, 25.4 mM) were sequentially added. The color of the solution immediately changed from light pink to orange and slowly to black after 1 h. The reaction lasted for 6 h. Au superparticles were then collected by centrifugation and redispersed in deionized water. We also prepared Au superparticles with different reaction times (3, 6, 8, and 12 h) for screening Au superparticles with a high degree of branching and good photothermal properties.

Synthesis of Au NRs. The synthesis of Au NRs started from the synthesis of Au seeds. $HAuCl_4$ solution (0.01 M, 250 μL) was added to 10 mL of cetyltrimethylammonium bromide (CTAB) solution (0.1 M). Then, 0.6 mL of $NaBH_4$ solution (0.01 M) was added, and the mixture was stirred for 2 min. The color of the solution changed from orange to light brown, indicating the formation of Au seeds. For the synthesis of Au NRs, 1.445 g of CTAB was dissolved in 40 mL of deionized water and heated to 45 °C. After the mixture was cooled to room temperature, 2 mL of $HAuCl_4$ solution (0.01 M) and 0.8 mL of HCl solution (1 M) were added to the CTAB solution and shaken for 30 s to form a homogeneous mixture. Then, 0.4 mL of a $AgNO_3$ solution (0.01 M) and 0.32 mL of an ascorbic acid solution (0.1 M) were added and shaken for 30 s. Finally, 0.096 mL of Au seed solution was added to the above solution and shaken for 30 s. The mixture was placed in a water bath at 35 °C for 16 h to promote the growth of Au NRs. The formed Au NRs were separated from the solution by centrifugation (10,000 rpm) and redispersed in deionized water. The purification step was repeated three times before the Au NRs were dispersed in water for further use.

Calculation of Photothermal Conversion Efficiency of Au Superparticles and NRs. Dispersions of Au superparticles (12.5−100 ppm) and Au NRs (100 ppm) were prepared for the measurements and estimation of their photothermal conversion efficiency. An 808 nm laser with a power density of 10 mW/mm^2 and a spot radius of 2 mm was used as the light source, and the temperature was recorded by an infrared camera. The photothermal conversion efficiency (η) of samples was calculated based on data shown in Figure 2a using the Roper's method.[54,55]

$$\eta = \frac{Hs(T_{max} - T_{surr}) - Q_{dis}}{I(1 - 10^{-A_{808}})} \quad (1)$$

In eq 1, H is the heat transfer coefficient, s is the surface area of the container, T_{max} is the maximum temperature of the nanomaterial dispersion after irradiation, T_{surr} is the environmental/surrounding temperature (15.2 °C in our experiment), Q_{dis} is the laser heat absorbed by the quartz cuvette (negligible), I is the laser power density (10 mW/mm^2), and A_{808} is the optical absorbance of Au superparticles or NRs at 808 nm. While other parameters were directly measured, the product of Hs can be estimated from the plot of temperature changes, according to eqs 2−4.

$$Hs = \frac{mC}{\tau_s} \quad (2)$$

$$\tau_s = \frac{t}{-\ln(\theta)} \quad (3)$$

$$\theta = \frac{T - T_{surr}}{T_{max} - T_{surr}} \quad (4)$$

In eq 2, m is the mass of the dispersion, C is the heat capacity of water (4.2 J/g), and τ_s is the time constant for heat transfer of the samples measured from the cooling curve. As shown in eq 3, to calculate τ_s, one can use the cooling time (t) and θ, which is defined in eq 4. In eq 4, T is the real-time temperature measured during cooling.

Measurement of the Transient Temperature Increases Induced by Au Superparticle Films. Voltage clamp setups with a diaphragm clamp amplifier were used for measuring the transient temperature increases in film samples. The resistance of the glass electrodes in phosphate-buffered solution (PBS, 4 mL, 0.01 M, containing Na_2HPO_4, KH_2PO_4, NaCl, and KCl, purchased from Solarbio) was approximately 1−2 MΩ. Sample films were prepared by spin coating solutions of Au NRs or superparticles (100 ppm) on 1 cm × 1 cm quartz substrates. The films were soaked in PBS solution (0.1 M) in a Petri dish with the glass electrode placed close to the surface of films. During irradiation, the temperature near the film surface increased, which changed the current ($\Delta I_{thermal}$) between the glass electrode and the Ag/AgCl electrode (also immersed in the solution). $\Delta I_{thermal}$ can be expressed by the following eq 5:

$$\Delta I_{thermal} = \left(\frac{R_0}{R_t} - 1\right) \times I_0 \quad (5)$$

where R_0 and R_t are the resistance of the glass electrode at room temperature and after laser irradiation, respectively, and I_0 is the dark current. R_0 was set to be 3−5 MΩ. The ratio of R_0 and R_t can then be

https://doi.org/10.1021/acsnano.4c07163
ACS Nano 2024, 18, 29572−29584

used to estimate the temperature near the film samples based on the Arrhenius's law (eq 6), where A is the slope of the calibration curve, T is the heating temperature and, and C' is the calibration curve intercept.

$$\ln\left(\frac{R_t}{R_0}\right) = \frac{A}{T} + C' \tag{6}$$

In our experiment, to calibrate the relationship between glass electrode resistance ($\Delta I_{thermal}$ or R_t/R_0) and temperature (T), we heated the PBS solution (0.1 M, 4 mL) to 53 °C and measured the resistance changes during the cooling of solution (Figure.S4). This allowed the extraction of A and C'. Based on these constants and eq 6, we can then estimate the temperature increases induced by Au nanomaterial or dopamine films when irradiated at different laser power densities (130−590 mW/mm^2).

Preparation of Film Samples for the Photothermal Modulation of Cells. Solutions of Au branched superparticles or NRs (100 ppm in ethanol) were spin-coated at 1200 rpm on quartz substrates (1 cm × 1 cm) and dried naturally before cell culturing.

Cell Culture. For primary mouse hippocampal neurons, a hippocampal tissue was dissected from P0 mice with Hank's balanced salt solution containing 4-(2-hydroxyethyl)-1-piperazineethanesulfonic acid (HEPES, 5 mM) and D-glucose (20 mM) under a dissecting microscope, digested with trypsin (0.25%) for 10 min at 37 °C, and washed with Dulbecco's modified Eagle's medium (DMEM) containing fetal bovine serum (FBS, 2%). The isolated cells were cultured in Neurobasal A containing B27 (2%), GlutaMax (2 mM), and penicillin−streptomycin (P/S, 1%). The Au branched superparticle films were sterilized with ethanol (70%) and irradiated under UV for 30 min followed by immersion in a solution of poly-D-lysine (0.25 mg/mL) for 8 h. The hippocampal neurons were then incubated on sample films for 7 days at a density of 50,000−100,000 cells/cm^2.

We also cultured other cells (such as PC-12 and MCF7) on films of Au superparticles or NRs for comparing their photothermal stimulation efficacy. MCF7 cells were washed three times with a 1× PBS solution, digested with 0.25% trypsin for 2 min (37 °C, 5 °C CO_2), and centrifuged at 1000 rpm for 3 min. After discarding the supernatant, a fresh medium (Dulbecco's modified Eagle's medium (DMEM) with high glucose, supplemented with 10% FBS and 1% P/S) was added, and the cells were dispersed and incubated on sterilized Au superparticle or NR films for 24 h. PC-12 cells were incubated following similar procedures except for using a different medium (Roswell Park Memorial Institute 1640 medium without L-glutamine, 10% FBS, and 1% P/S).

Cell Biocompatibility Assay and Immunofluorescence Imaging. To test the activity of primary mouse hippocampal neurons cultured on Au superparticle films, fluorescence imaging tests were performed by using a LIVE/DEAD cell imaging kit (488/570). After being washed with Hank's balanced salt solution with 20 mM HEPES buffer (HHBS) solution three times, live cells, dead cells, and nuclei were labeled with Calcein AM (green), EthD-1 (red), and Hoechst33342 (blue), respectively. After the cells were incubated in the dye solution for 15 min at room temperature, images were taken with a Nikon AXR NSPARC confocal microscope. We also performed similar cell viability tests on mouse hippocampal neurons cultured on Au superparticle films after laser irradiation, as shown in Figure S11.

For the c-Fos immunofluorescence imaging, cells were washed three times with 1× PBS, fixed with paraformaldehyde, washed with PBS, permeabilized with Triton X-100, washed with PBS, and then blocked with 5% BSA. Cells were then incubated with a primary antibody (anti-c-Fos antibody) overnight at 4 °C. After removing excess liquid, cells were washed with PBS with Tween-20 followed by incubation in a fluorescent secondary antibody (IgG H&L with Alexa Fluor 594) for 1 h at room temperature. Cells were then washed with PBS with Tween-20 and added with an antifade mounting medium with DAPI for subsequent imaging.

Calcium Imaging for Evaluating the Neural Modulation Efficacy. Primary mouse hippocampal neurons cultured on Au superparticle films were stained with Calbryte 520 as a fluorescent calcium indicator. In brief, 50 μg of Calbryte 520 AM was dissolved in 45.8 μL of dimethyl sulfoxide (DMSO) and stored at −20 °C. Cells were washed three times with HHBS solution, incubated in a solution (4 μL of the Calbryte 520 solution in DMSO dissolved in 1 mL of HHBS buffer) for 30 min, washed three times, and then incubated in HHBS solution for 30 min. Calcium imaging was performed with a Nikon A1RMP multiphoton confocal microscope. The stimulation laser was tuned to 800 nm (Mai Tai DeepSee, Spectra-Physics), while another laser (488 nm) was used to image the region of interest. Prior to stimulation, the fluorescence images were captured for ∼50 s to collect the baseline. The 800 nm laser was then turned on in resonance mode, and the fluorescence images were taken for the stimulated neurons for 10 s. The 800 nm laser has a full power of 196 mW. The laser power can be tuned to be a certain percentage of the full power (e.g., 12, 8, 4, 2, and 1%, corresponding to ∼24, 16, 8, 4, and 2 mW, respectively). The changes of the fluorescence intensities of Calbryte 520 indicators during the process were analyzed by using ImageJ software.

For comparing the photothermal stimulation efficiency of Au superparticles and NRs, we imaged stained PC-12 cells (stained with Calbryte 520) using a Nikon A1R confocal microscope with a 20× objective and a 488 nm solid-state laser. In this case, an external 808 nm laser (55.2 mW/mm^2) was used to trigger the photothermal behavior of Au superparticle or NR films, and the 488 nm laser was used for fluorescence imaging. Similar to the case of primary mouse hippocampal neurons, we collected the images for about 1 min before turning on the 808 nm laser. Then, the calcium fluorescence of cultured PC-12 cells under photostimulation was monitored for 1 min. Afterward, additional images were captured for 3 min to collect the data for cells after stimulation.

Whole-Cell Membrane Clamp Assay for Demonstrating the Suppression of Neuronal Activity. Primary mouse hippocampal neurons were cultured on Au superparticle films using the procedures described above. Utilizing a MultiClamp 700B amplifier (Molecular Devices), whole-cell recordings were performed in the current-clamp mode. During the experiments, neurons were perfused with a solution (containing 128 mM NaCl, 30 mM glucose, 5 mM KCl, 2 mM $CaCl_2$, 1 mM $MgCl_2$, and 25 mM HEPES, pH 7.3) at room temperature. Patch pipettes made of borosilicate glass were filled with an internal solution (containing 130 mM K-gluconate, 1 mM ethylene glycol-bis(β-aminoethyl ether)-*N*,*N*,*N*′,*N*′-tetraacetic acid (EGTA), 5 mM Na-phosphocreatine, 2 mM Mg-ATP, 0.3 mM Na-GTP, and 10 mM HEPES, pH 7.3), with a resistance ranging from 3 to 5 MΩ. The series resistance was typically <15 MΩ.

To show the suppression of neural activity, we first injected positive currents to keep neurons at the desired membrane potential (−55 mV) to evoke action potentials. Then, the Au superparticle films were irradiated with an 808 nm laser (10, 4.3, 2.7 mW/mm^2, 15 s) mode. During the process, changes in the neuronal membrane potential were collected with a current clamp and recorded with pClamp10 software (Molecular Devices) with low-pass filtering at 2 kHz and a sampling frequency of 10 kHz. The data were analyzed using Clampfit software (Molecular Devices).

Characterization Techniques. HRTEM and EDS analysis was performed on a Hitachi JEM2010. FTIR spectra of films were collected using a Bruker VERTEX 70 spectrometer in transmission mode. TGA analysis of Au superparticles was performed by using a Mettler Toledo TGA/DSC 1 HT/1600 instrument at a heating rate of 3 °C/min.

TEM images of Au superparticles and NRs were captured with a Hitachi H-7700 microscope. Optical absorption spectra of the nanomaterials were measured by an Agilent Cary-5000 UV−vis−NIR spectrophotometer. Changes in the solution temperature were recorded using a Fluke Ti400 infrared thermal imaging camera. Fluorescence imaging for cell viability and c-Fos immunology was carried out using a Nikon AXR NSPARC laser scanning confocal microscope. Calcium imaging of primary hippocampal neurons cultured on Au superparticle films was performed on a Nikon A1RMP multiphoton confocal microscope, where a Mai Tai laser

https://doi.org/10.1021/acsnano.4c07163
ACS Nano 2024, 18, 29572−29584

(800 nm, full power, 196 mW, Spectra-Physics) was used to stimulate the neurons. The laser power can be tuned to a certain percentage of the full power. Calcium imaging of PC-12 cells cultured on Au superparticle or Au NR films was conducted with a Nikon A1R confocal microscope. An external 808 nm laser (Hitech Photonics LOS-BLD-0808-005W-C/P) was used as the excitation source. For the whole-cell membrane clamp assay, the 808 nm laser mentioned above was used as the light source. The output power of the 808 nm laser was measured with a Thorlabs PM100D digital optical power and energy meter. Whole-cell recordings were performed with a MultiClamp 700B amplifier (Molecular Devices) and pClamp10 software (Molecular Devices).

ASSOCIATED CONTENT

Supporting Information

The Supporting Information is available free of charge at https://pubs.acs.org/doi/10.1021/acsnano.4c07163.

Structures and characterization of photothermal properties of Au superparticles and Au NRs; morphology of Au superparticle films; patch clamp temperature calibration curve; temperature increases induced by dopamine films; morphology, photothermal properties, and colloidal stability of Au superparticles with different reaction times; cell biocompatibility of MCF7 cells cultured on Au superparticle films; photothermal modulation of neuronal activities with different laser powers; confocal images depicting the expression of c-Fos in hippocampal neurons; cell viability of neurons after photothermal modulation; photothermal modulation of neurons cultured on dopamine films; photothermal modulation of PC-12 cell activities on Au superparticle and NR films; photothermal modulation of MCF7 cell activities by Au superparticle films with different laser powers; modulation of targeted neurons on Au superparticle films and quartz substrates; modulation of targeted MCF7 cells cultured on Au superparticle films with different laser powers; additional membrane potential recordings of neurons during photothermal inhibition and delay time statistics; whole-cell patch clamp recordings of mouse hippocampal neurons on quartz substrates and statistics (PDF)

Movie S1: Ca^{2+} influx through photothermal stimulation of mouse hippocampal neurons with different laser powers (MP4)

Movie S2: Ca^{2+} influx through modulation of target neurons with different laser powers (MP4)

AUTHOR INFORMATION

Corresponding Authors

Kangkang Weng − *Department of Chemistry, Center for Bioanalytical Chemistry, Key Laboratory of Bioorganic Phosphorus Chemistry & Chemical Biology (Ministry of Education), Tsinghua University, Beijing 100084, China; School of Optics and Photonics, Beijing Key Laboratory for Precision Optoelectronic Measurement Instrument and Technology, Beijing Institute of Technology, Beijing 100081, China; Yangtze Delta Region Academy of Beijing Institute of Technology, Jiaxing 314019, China*; Email: kangkangweng@bit.edu.cn

Jun Yao − *School of Life Sciences, State Key Laboratory of Membrane Biology, Tsinghua-Peking Center for Life Sciences, IDG/McGovern Institute for Brain Research, Tsinghua University, Beijing 100084, China*; Email: jyao@mail.tsinghua.edu.cn

Hao Zhang − *Department of Chemistry, Center for Bioanalytical Chemistry, Key Laboratory of Bioorganic Phosphorus Chemistry & Chemical Biology (Ministry of Education), Tsinghua University, Beijing 100084, China*; orcid.org/0000-0003-4513-0813; Email: hzhangchem@mail.tsinghua.edu.cn

Jinghong Li − *Department of Chemistry, Center for Bioanalytical Chemistry, Key Laboratory of Bioorganic Phosphorus Chemistry & Chemical Biology (Ministry of Education), Tsinghua University, Beijing 100084, China*; orcid.org/0000-0002-0750-7352; Email: jhli@mail.tsinghua.edu.cn

Authors

Xinyu Cheng − *Department of Chemistry, Center for Bioanalytical Chemistry, Key Laboratory of Bioorganic Phosphorus Chemistry & Chemical Biology (Ministry of Education), Tsinghua University, Beijing 100084, China*

Wenjun Li − *Department of Chemistry, Center for Bioanalytical Chemistry, Key Laboratory of Bioorganic Phosphorus Chemistry & Chemical Biology (Ministry of Education), Tsinghua University, Beijing 100084, China*

Yinghan Wang − *School of Life Sciences, State Key Laboratory of Membrane Biology, Tsinghua-Peking Center for Life Sciences, IDG/McGovern Institute for Brain Research, Tsinghua University, Beijing 100084, China*

Yunyun Xing − *School of Life Sciences, State Key Laboratory of Membrane Biology, Tsinghua-Peking Center for Life Sciences, IDG/McGovern Institute for Brain Research, Tsinghua University, Beijing 100084, China*

Yunxiang Huang − *Department of Electronic Engineering, Beijing National Research Center for Information Science and Technology, Institute for Precision Medicine, Laboratory of Flexible Electronics Technology, IDG/McGovern Institute for Brain Research, Tsinghua University, Beijing 100084, China*

Xing Sheng − *Department of Electronic Engineering, Beijing National Research Center for Information Science and Technology, Institute for Precision Medicine, Laboratory of Flexible Electronics Technology, IDG/McGovern Institute for Brain Research, Tsinghua University, Beijing 100084, China*; orcid.org/0000-0002-8744-1700

Complete contact information is available at: https://pubs.acs.org/10.1021/acsnano.4c07163

Author Contributions

[‖]X.C., W.L., and Y.W. contributed equally. The manuscript was written through contributions of all authors. All authors have given approval to the final version of the manuscript.

Notes

The authors declare no competing financial interest.

ACKNOWLEDGMENTS

This work was supported by the National Key Research and Development Program of China (no. 2022YEA1206101, H.Z., and no. 2021YFA1200104, J.L.), the National Natural Science Foundation of China (no. 22274087, H.Z.), the Tsinghua University Dushi Program (H.Z.), the China Postdoctoral Science Foundation (nos. 2021TQ0168 and 2021M691758, K.W.), and the 2022 Doctoral/Postdoctoral Project Applica-

tion Report For "Brain+X" Seed Grant Program (Y.W. and K.W.).

REFERENCES

(1) Zimmerman, J. F.; Tian, B. Nongenetic Optical Methods for Measuring and Modulating Neuronal Response. *ACS Nano* **2018**, *12* (5), 4086−4095.
(2) Vázquez-Guardado, A.; Yang, Y.; Bandodkar, A. J.; Rogers, J. A. Recent advances in neurotechnologies with broad potential for neuroscience research. *Nat. Neurosci.* **2020**, *23* (12), 1522−1536.
(3) Rivnay, J.; Wang, H.; Fenno, L.; Deisseroth, K.; Malliaras, G. G. Next-generation probes, particles, and proteins for neural interfacing. *Sci. Adv.* **2017**, *3* (6), No. e1601649.
(4) Lozano, A. M.; Lipsman, N.; Bergman, H.; Brown, P.; Chabardes, S.; Chang, J. W.; Matthews, K.; McIntyre, C. C.; Schlaepfer, T. E.; Schulder, M.; et al. Deep brain stimulation: current challenges and future directions. *Nat. Rev. Neurol.* **2019**, *15* (3), 148−160.
(5) Salatino, J. W.; Ludwig, K. A.; Kozai, T. D. Y.; Purcell, E. K. Glial responses to implanted electrodes in the brain. *Nat. Biomed. Eng.* **2017**, *1* (11), 862−877.
(6) Boyden, E. S.; Zhang, F.; Bamberg, E.; Nagel, G.; Deisseroth, K. Millisecond-timescale, genetically targeted optical control of neural activity. *Nat. Neurosci.* **2005**, *8* (9), 1263−1268.
(7) Deisseroth, K. Optogenetics. *Nat. Methods* **2011**, *8* (1), 26−29.
(8) Carvalho-de-Souza, J. L.; Treger, J. S.; Dang, B.; Kent, S. B. H.; Pepperberg, D. R.; Bezanilla, F. Photosensitivity of Neurons Enabled by Cell-Targeted Gold Nanoparticles. *Neuron* **2015**, *86* (1), 207−217.
(9) Williams, J. C.; Denison, T. From Optogenetic Technologies to Neuromodulation Therapies. *Sci. Transl. Med.* **2013**, *5* (177), 177ps6.
(10) Tian, B. Nongenetic neural control with light. *Science* **2019**, *365* (6452), 457−457.
(11) Jiang, Y.; Tian, B. Inorganic semiconductor biointerfaces. *Nat. Rev. Mater.* **2018**, *3* (12), 473−490.
(12) Ghezzi, D.; Antognazza, M. R.; Dal Maschio, M.; Lanzarini, E.; Benfenati, F.; Lanzani, G. A hybrid bioorganic interface for neuronal photoactivation. *Nat. Commun.* **2011**, *2* (1), 166.
(13) Fang, Y.; Meng, L.; Prominski, A.; Schaumann, E. N.; Seebald, M.; Tian, B. Recent advances in bioelectronics chemistry. *Chem. Soc. Rev.* **2020**, *49* (22), 7978−8035.
(14) Fang, Y.; Yang, X.; Lin, Y.; Shi, J.; Prominski, A.; Clayton, C.; Ostroff, E.; Tian, B. Dissecting Biological and Synthetic Soft−Hard Interfaces for Tissue-Like Systems. *Chem. Rev.* **2022**, *122* (5), 5233−5276.
(15) Simon, D. T.; Gabrielsson, E. O.; Tybrandt, K.; Berggren, M. Organic Bioelectronics: Bridging the Signaling Gap between Biology and Technology. *Chem. Rev.* **2016**, *116* (21), 13009−13041.
(16) Jiang, Y.; Li, X.; Liu, B.; Yi, J.; Fang, Y.; Shi, F.; Gao, X.; Sudzilovsky, E.; Parameswaran, R.; Koehler, K.; et al. Rational design of silicon structures for optically controlled multiscale biointerfaces. *Nat. Biomed. Eng.* **2018**, *2* (7), 508−521.
(17) Jiang, Y.; Carvalho-de-Souza, J. L.; Wong, R. C. S.; Luo, Z.; Isheim, D.; Zuo, X.; Nicholls, A. W.; Jung, I. W.; Yue, J.; Liu, D.-J.; et al. Heterogeneous silicon mesostructures for lipid-supported bioelectric interfaces. *Nat. Mater.* **2016**, *15* (9), 1023−1030.
(18) Silverå Ejneby, M.; Jakešová, M.; Ferrero, J. J.; Migliaccio, L.; Sahalianov, I.; Zhao, Z.; Berggren, M.; Khodagholy, D.; Đerek, V.; Gelinas, J. N.; et al. Chronic electrical stimulation of peripheral nerves via deep-red light transduced by an implanted organic photocapacitor. *Nat. Biomed. Eng.* **2022**, *6* (6), 741−753.
(19) Rand, D.; Jakešová, M.; Lubin, G.; Vėbraitė, I.; David-Pur, M.; Đerek, V.; Cramer, T.; Sariciftci, N. S.; Hanein, Y.; Głowacki, E. D. Direct Electrical Neurostimulation with Organic Pigment Photocapacitors. *Adv. Mater.* **2018**, *30* (25), No. 1707292.
(20) Cui, H.; Zhao, S.; Hong, G. Wireless deep-brain neuromodulation using photovoltaics in the second near-infrared spectrum. *Device* **2023**, *1* (4), No. 100113.
(21) Karatum, O.; Kaleli, H. N.; Eren, G. O.; Sahin, A.; Nizamoglu, S. Electrical Stimulation of Neurons with Quantum Dots via Near-Infrared Light. *ACS Nano* **2022**, *16* (5), 8233−8243.
(22) Bahmani Jalali, H.; Mohammadi Aria, M.; Dikbas, U. M.; Sadeghi, S.; Ganesh Kumar, B.; Sahin, M.; Kavakli, I. H.; Ow-Yang, C. W.; Nizamoglu, S. Effective Neural Photostimulation Using Indium-Based Type-II Quantum Dots. *ACS Nano* **2018**, *12* (8), 8104−8114.
(23) Yoo, S.; Kim, R.; Park, J.-H.; Nam, Y. Electro-optical Neural Platform Integrated with Nanoplasmonic Inhibition Interface. *ACS Nano* **2016**, *10* (4), 4274−4281.
(24) Martino, N.; Feyen, P.; Porro, M.; Bossio, C.; Zucchetti, E.; Ghezzi, D.; Benfenati, F.; Lanzani, G.; Antognazza, M. R. Photothermal cellular stimulation in functional bio-polymer interfaces. *Sci. Rep.* **2015**, *5* (1), 8911.
(25) Abdullaeva, O. S.; Balzer, F.; Schulz, M.; Parisi, J.; Lützen, A.; Dedek, K.; Schiek, M. Organic Photovoltaic Sensors for Photocapacitive Stimulation of Voltage-Gated Ion Channels in Neuroblastoma Cells. *Adv. Funct. Mater.* **2019**, *29* (21), No. 1805177.
(26) Maya-Vetencourt, J. F.; Ghezzi, D.; Antognazza, M. R.; Colombo, E.; Mete, M.; Feyen, P.; Desii, A.; Buschiazzo, A.; Di Paolo, M.; Di Marco, S.; et al. A fully organic retinal prosthesis restores vision in a rat model of degenerative blindness. *Nat. Mater.* **2017**, *16* (6), 681−689.
(27) Jakešová, M.; Silverå Ejneby, M.; Đerek, V.; Schmidt, T.; Gryszel, M.; Brask, J.; Schindl, R.; Simon, D. T.; Berggren, M.; Elinder, F.; Głowacki, E. D.; et al. Optoelectronic control of single cells using organic photocapacitors. *Sci. Adv.* **2019**, *5* (4), No. eaav5265.
(28) Ferlauto, L.; Airaghi Leccardi, M. J. I.; Chenais, N. A. L.; Gilliéron, S. C. A.; Vagni, P.; Bevilacqua, M.; Wolfensberger, T. J.; Sivula, K.; Ghezzi, D. Design and validation of a foldable and photovoltaic wide-field epiretinal prosthesis. *Nat. Commun.* **2018**, *9* (1), 992.
(29) Bahmani Jalali, H.; Karatum, O.; Melikov, R.; Dikbas, U. M.; Sadeghi, S.; Yildiz, E.; Dogru, I. B.; Ozgun Eren, G.; Ergun, C.; Sahin, A.; et al. Biocompatible Quantum Funnels for Neural Photostimulation. *Nano Lett.* **2019**, *19* (9), 5975−5981.
(30) Parameswaran, R.; Tian, B. Scalable breakthrough. *Nat. Nanotechnol.* **2018**, *13* (10), 875−876.
(31) Benfenati, V.; Martino, N.; Antognazza, M. R.; Pistone, A.; Toffanin, S.; Ferroni, S.; Lanzani, G.; Muccini, M. Photostimulation of Whole-Cell Conductance in Primary Rat Neocortical Astrocytes Mediated by Organic Semiconducting Thin Films. *Adv. Healthcare Mater.* **2014**, *3* (3), 392−399.
(32) Tortiglione, C.; Antognazza, M. R.; Tino, A.; Bossio, C.; Marchesano, V.; Bauduin, A.; Zangoli, M.; Morata, S. V.; Lanzani, G. Semiconducting polymers are light nanotransducers in eyeless animals. *Sci. Adv.* **2017**, *3* (1), No. e1601699.
(33) Huang, H.; Delikanli, S.; Zeng, H.; Ferkey, D. M.; Pralle, A. Remote control of ion channels and neurons through magnetic-field heating of nanoparticles. *Nat. Nanotechnol.* **2010**, *5* (8), 602−606.
(34) Zhang, H.; Huang, H.; He, S.; Zeng, H.; Pralle, A. Monodisperse magnetofluorescent nanoplatforms for local heating and temperature sensing. *Nanoscale* **2014**, *6* (22), 13463−13469.
(35) Yang, C.; Park, S. Nanomaterials-assisted thermally induced neuromodulation. *Biomed. Eng. Lett.* **2021**, *11* (3), 163−170.
(36) Huang, X.; Neretina, S.; El-Sayed, M. A. Gold Nanorods: From Synthesis and Properties to Biological and Biomedical Applications. *Adv. Mater.* **2009**, *21* (48), 4880−4910.
(37) Li, N.; Zhao, P.; Astruc, D. Anisotropic Gold Nanoparticles: Synthesis, Properties, Applications, and Toxicity. *Angew. Chem., Int. Ed.* **2014**, *53* (7), 1756−1789.
(38) Yoo, S.; Hong, S.; Choi, Y.; Park, J.-H.; Nam, Y. Photothermal Inhibition of Neural Activity with Near-Infrared-Sensitive Nanotransducers. *ACS Nano* **2014**, *8* (8), 8040−8049.
(39) Carvalho-de-Souza, J. L.; Pinto, B. I.; Pepperberg, D. R.; Bezanilla, F. Optocapacitive Generation of Action Potentials by Microsecond Laser Pulses of Nanojoule Energy. *Biophys. J.* **2018**, *114* (2), 283−288.

https://doi.org/10.1021/acsnano.4c07163
ACS Nano 2024, 18, 29572−29584

(40) Kang, H.; Hong, W.; An, Y.; Yoo, S.; Kwon, H.-J.; Nam, Y. Thermoplasmonic Optical Fiber for Localized Neural Stimulation. *ACS Nano* **2020**, *14* (9), 11406−11419.
(41) Jang, H.; Yoon, D.; Nam, Y. Enhancement of Thermoplasmonic Neural Modulation Using a Gold Nanorod-Immobilized Polydopamine Film. *ACS Appl. Mater.* **2022**, *14* (21), 24122−24132.
(42) Yoo, S.; Park, J.-H.; Nam, Y. Single-Cell Photothermal Neuromodulation for Functional Mapping of Neural Networks. *ACS Nano* **2019**, *13* (1), 544−551.
(43) Savchenko, A.; Cherkas, V.; Liu, C.; Braun, G. B.; Kleschevnikov, A.; Miller, Y. I.; Molokanova, E. Graphene biointerfaces for optical stimulation of cells. *Sci. Adv.* **2018**, *4* (5), No. eaat0351.
(44) Rastogi, S. K.; Garg, R.; Scopelliti, M. G.; Pinto, B. I.; Hartung, J. E.; Kim, S.; Murphey, C. G. E.; Johnson, N.; San Roman, D.; Bezanilla, F.; et al. Remote nongenetic optical modulation of neuronal activity using fuzzy graphene. *Proc. Natl. Acad. Sci. U.S.A.* **2020**, *117* (24), 13339−13349.
(45) Shao, L.; Wei, H.; Liu, J.; Ma, W.; Yu, P.; Wang, M.; Mao, L. Graphdiyne as a Highly Efficient and Neuron-Targeted Photothermal Transducer for in Vivo Neuromodulation. *ACS Nano* **2024**, *18* (24), 15607−15616.
(46) Fang, Y.; Jiang, Y.; Acaron Ledesma, H.; Yi, J.; Gao, X.; Weiss, D. E.; Shi, F.; Tian, B. Texturing Silicon Nanowires for Highly Localized Optical Modulation of Cellular Dynamics. *Nano Lett.* **2018**, *18* (7), 4487−4492.
(47) Wang, Y.; Garg, R.; Hartung, J. E.; Goad, A.; Patel, D. A.; Vitale, F.; Gold, M. S.; Gogotsi, Y.; Cohen-Karni, T. Ti3C2Tx MXene Flakes for Optical Control of Neuronal Electrical Activity. *ACS Nano* **2021**, *15* (9), 14662−14671.
(48) Zhong, Q.; Feng, J.; Jiang, B.; Fan, Y.; Zhang, Q.; Chen, J.; Yin, Y. Strain-Modulated Seeded Growth of Highly Branched Black Au Superparticles for Efficient Photothermal Conversion. *J. Am. Chem. Soc.* **2021**, *143* (48), 20513−20523.
(49) Kwon, N.; Oh, H.; Kim, R.; Sinha, A.; Kim, J.; Shin, J.; Chon, J. W. M.; Lim, B. Direct Chemical Synthesis of Plasmonic Black Colloidal Gold Superparticles with Broadband Absorption Properties. *Nano Lett.* **2018**, *18* (9), 5927−5932.
(50) Wang, C.; Zhou, L.; Liu, C.; Qiao, J.; Han, X.; Wang, L.; Liu, Y.; Xu, B.; Qiu, Q.; Zhang, Z.; et al. Pt nanoshells with a high NIR-II photothermal conversion efficiency mediates multimodal neuromodulation against ventricular arrhythmias. *Nat. Commun.* **2024**, *15* (1), 6362.
(51) Hong, N.; Nam, Y. Thermoplasmonic neural chip platform for in situ manipulation of neuronal connections in vitro. *Nat. Commun.* **2020**, *11* (1), 6313.
(52) Chen, J.; Feng, J.; Li, Z.; Xu, P.; Wang, X.; Yin, W.; Wang, M.; Ge, X.; Yin, Y. Space-Confined Seeded Growth of Black Silver Nanostructures for Solar Steam Generation. *Nano Lett.* **2019**, *19* (1), 400−407.
(53) Zhou, L.; Tan, Y.; Wang, J.; Xu, W.; Yuan, Y.; Cai, W.; Zhu, S.; Zhu, J. 3D self-assembly of aluminium nanoparticles for plasmon-enhanced solar desalination. *Nat. Photonics* **2016**, *10* (6), 393−398.
(54) Wang, Y.; Gong, N.; Li, Y.; Lu, Q.; Wang, X.; Li, J. Atomic-Level Nanorings (A-NRs) Therapeutic Agent for Photoacoustic Imaging and Photothermal/Photodynamic Therapy of Cancer. *J. Am. Chem. Soc.* **2020**, *142* (4), 1735−1739.
(55) Roper, D. K.; Ahn, W.; Hoepfner, M. Microscale Heat Transfer Transduced by Surface Plasmon Resonant Gold Nanoparticles. *J. Phys. Chem. C* **2007**, *111* (9), 3636−3641.
(56) Eom, K.; Byun, K. M.; Jun, S. B.; Kim, S. J.; Lee, J. Theoretical Study on Gold-Nanorod-Enhanced Near-Infrared Neural Stimulation. *Biophys. J.* **2018**, *115* (8), 1481−1497.
(57) Kang, H.; Lee, G.-H.; Jung, H.; Lee, J. W.; Nam, Y. Inkjet-Printed Biofunctional Thermo-Plasmonic Interfaces for Patterned Neuromodulation. *ACS Nano* **2018**, *12* (2), 1128−1138.
(58) Chen, H.; Shao, L.; Ming, T.; Sun, Z.; Zhao, C.; Yang, B.; Wang, J. Understanding the Photothermal Conversion Efficiency of Gold Nanocrystals. *Small* **2010**, *6* (20), 2272−2280.
(59) Kim, H. S.; Lee, D. Y. Near-Infrared-Responsive Cancer Photothermal and Photodynamic Therapy Using Gold Nanoparticles. *Polymers* **2018**, *10* (9), 961.
(60) Lee, J. W.; Jung, H.; Cho, H. H.; Lee, J. H.; Nam, Y. Gold nanostar-mediated neural activity control using plasmonic photothermal effects. *Biomaterials* **2018**, *153*, 59−69.
(61) Alkilany, A. M.; Nagaria, P. K.; Hexel, C. R.; Shaw, T. J.; Murphy, C. J.; Wyatt, M. D. Cellular Uptake and Cytotoxicity of Gold Nanorods: Molecular Origin of Cytotoxicity and Surface Effects. *Small* **2009**, *5* (6), 701−708.
(62) Kirui, D. K.; Krishnan, S.; Strickland, A. D.; Batt, C. A. PAA-Derived Gold Nanorods for Cellular Targeting and Photothermal Therapy. *Macromol. Biosci.* **2011**, *11* (6), 779−788.
(63) Ye, T.; Lai, Y.; Wang, Z.; Zhang, X.; Meng, G.; Zhou, L.; Zhang, Y.; Zhou, Z.; Deng, J.; Wang, M.; et al. Precise Modulation of Gold Nanorods for Protecting against Malignant Ventricular Arrhythmias via Near-Infrared Neuromodulation. *Adv. Funct. Mater.* **2019**, *29* (36), No. 1902128.
(64) Christie, J. M.; Chiu, D. N.; Jahr, C. E. Ca^{2+}-dependent enhancement of release by subthreshold somatic depolarization. *Nat. Neurosci.* **2011**, *14* (1), 62−68.
(65) Kamiya, H.; Zucker, R. S. Residual Ca^{2+} and short-term synaptic plasticity. *Nature* **1994**, *371* (6498), 603−606.
(66) Wu, X.; Jiang, Y.; Rommelfanger, N. J.; Yang, F.; Zhou, Q.; Yin, R.; Liu, J.; Cai, S.; Ren, W.; Shin, A.; et al. Tether-free photothermal deep-brain stimulation in freely behaving mice via wide-field illumination in the near-infrared-II window. *Nat. Biomed. Eng.* **2022**, *6* (6), 754−770.
(67) Brown, W. G. A.; Needham, K.; Begeng, J. M.; Thompson, A. C.; Nayagam, B. A.; Kameneva, T.; Stoddart, P. R. Thermal damage threshold of neurons during infrared stimulation. *Biomed. Opt. Express* **2020**, *11* (4), 2224−2234.
(68) Shoji-Kasai, Y.; Yoshida, A.; Sato, K.; Hoshino, T.; Ogura, A.; Kondo, S.; Fujimoto, Y.; Kuwahara, R.; Kato, R.; Takahashi, M. Neurotransmitter Release from Synaptotagmin-Deficient Clonal Variants of PC 12 Cells. *Science* **1992**, *256* (5065), 1820−1823.
(69) Zhu, D.; Feng, L.; Feliu, N.; Guse, A. H.; Parak, W. J. Stimulation of Local Cytosolic Calcium Release by Photothermal Heating for Studying Intra- and Intercellular Calcium Waves. *Adv. Mater.* **2021**, *33* (24), No. 2008261.
(70) Kohara, K.; Kitamura, A.; Morishima, M.; Tsumoto, T. Activity-Dependent Transfer of Brain-Derived Neurotrophic Factor to Postsynaptic Neurons. *Science* **2001**, *291* (5512), 2419−2423.
(71) Huang, Y.; Cui, Y.; Deng, H.; Wang, J.; Hong, R.; Hu, S.; Hou, H.; Dong, Y.; Wang, H.; Chen, J.; et al. Bioresorbable thin-film silicon diodes for the optoelectronic excitation and inhibition of neural activities. *Nat. Biomed. Eng.* **2023**, *7* (4), 486−498.

https://doi.org/10.1021/acsnano.4c07163
ACS Nano 2024, 18, 29572−29584

Supporting Information

Highly Branched Au Superparticles as Efficient Photothermal Transducers for Optical Neuromodulation

Xinyu Cheng,[†,⊥] Wenjun Li,[†,⊥] Yinghan Wang,[§,⊥] Kangkang Weng,[†,‡,#,] Yunyun Xing,[§] Yunxiang Huang,[ϟ] Xing Sheng,[ϟ] Jun Yao,[§,*] Hao Zhang,[†,*] Jinghong Li[†,*]*

[†]Department of Chemistry, Center for Bioanalytical Chemistry, Key Laboratory of Bioorganic Phosphorus Chemistry & Chemical Biology (Ministry of Education), Tsinghua University, Beijing 100084, China

[§]School of Life Sciences, State Key Laboratory of Membrane Biology, Tsinghua-Peking Center for Life Sciences, IDG/McGovern Institute for Brain Research, Tsinghua University, Beijing 100084, China

[‡]School of Optics and Photonics, Beijing Key Laboratory for Precision Optoelectronic Measurement Instrument and Technology, Beijing Institute of Technology, Beijing 100081, China

[#]Yangtze Delta Region Academy of Beijing Institute of Technology, Jiaxing 314019, China

ϟDepartment of Electronic Engineering, Beijing National Research Center for Information Science and Technology, Institute for Precision Medicine, Laboratory of Flexible Electronics Technology, IDG/McGovern Institute for Brain Research, Tsinghua University, Beijing 100084, China

*Email: kangkangweng@bit.edu.cn; jyao@mail.tsinghua.edu.cn;

hzhangchem@mail.tsinghua.edu.cn; jhli@mail.tsinghua.edu.cn

Chemicals. Tetrachloroauric acid trihydrate ($HAuCl_4 \cdot 3H_2O$, 99.9%), polyvinylpyrrolidone (PVP, M_w = 10000), potassium iodide (99%), sodium borohydride ($NaBH_4$, 99%), ascorbic acid (99%), trisodium citrate dihydrate (99%), dopamine (99%), hexadecyl trimethyl ammonium bromide (CTAB, 99%) and Tris hydrochloride (Tris-HCl) were purchased from Aladdin. Ethanol (AR) was purchased from BeiJing TongGuang. Hydrochloric acid (HCl) was purchased from Sinopharm. Sodium chloride (NaCl, 99%), magnesium chloride ($MgCl_2$, 99.99%), calcium chloride ($CaCl_2$, 96%), potassium chloride (KCl, 99%), sodium hydroxide (NaOH, 97%), 4-(2-hydroxyethyl)-1-piperazineethanesulfonic acid (HEPES, 99.5%), potassium D-gluconate (K-Gluconate, 99%), D-(+)-glucose (99.5%), ethylene glycol-bis(β-aminoethyl ether)-*N*,*N*,*N*′,*N*′-tetraacetic acid (EGTA, 97%), phosphocreatine disodium salt hydrate (Na-phosphocreatine, 97%), adenosine 5’-triphosphate magnesium salt (Mg-ATP, 95%), guanosine 5’-triphosphate sodium salt hydrate (Na-GTP, 95%) were purchased from Sigma-Aldrich. MCF7 cells were purchased from China National Infrastructure of Cell Line Resource. PC-12 (High differentiation) cells were purchased from Wuhan Pricella Biotechnology. Other reagents included Dulbecco's modified eagle’s medium (DMEM, Hyclone), Roswell Park Memorial Institute 1640 medium (Gibco), fetal bovine serum (FBS, EallBio), penicillin-streptomycin (P/S, Yeasen), trypsin-EDTA (0.25%, Yeasen), phosphate buffered solution (PBS, Solarbio, 0.01 M, containing Na_2HPO_4, KH_2PO_4, NaCl, and KCl), Neurobasal-A (Gibco), B27 (Gibco), GlutaMAX-I (Invitrogen), poly-D-lysine (Thermo Fisher), Calbryte-520 AM (AAT Bioquest), LIVE/DEAD™ cell imaging kit (Invitrogen), Hank's balanced salt solution

with 20 mM HEPES (HHBS, Maokangbio), anti-c-Fos antibody (abcam), IgG H&L (Alexa Fluor 594, abcam). All chemicals and biochemicals were used as received without further purification.

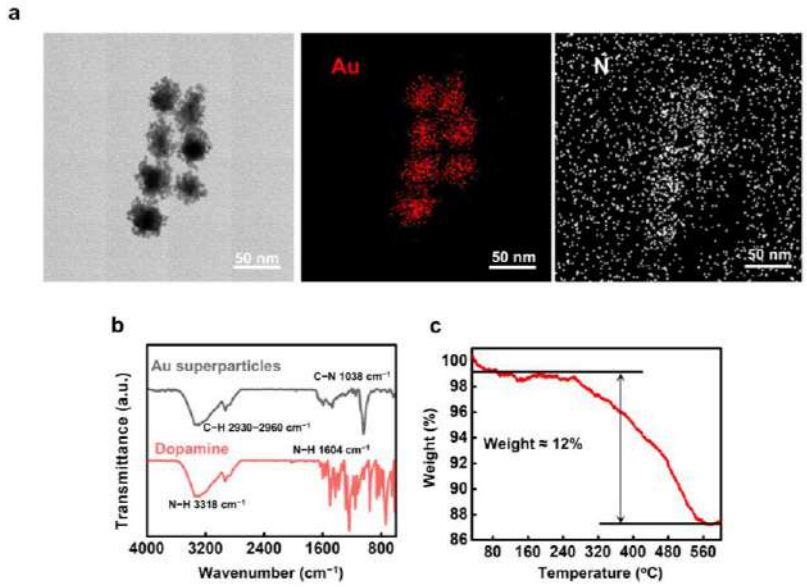

Figure S1. Additional characterization of Au superparticles. (a) High-resolution TEM image and EDS analysis of Au superparticles. **(b)** FTIR spectra and **(c)** TGA analysis of Au superparticles.

The HRTEM images show the branched structure of Au superparticles. The distribution of N elements mostly follows that of the Au superparticle cores. The FTIR spectra of Au superparticles show characteristic resonance peaks (N−H, C−H, C−N) corresponding to dopamine. The EDS and FTIR analysis confirm that the ligands of Au superparticles are polydopamine. The contents of polydopamine ligands (about 12% in weight to the sum of Au and polydopamine) in the Au superparticles can be estimated from TGA data. From this data, we can estimate the percentage of volume of pure Au in the superparticles and the density of Au superparticles by using the following equations (1 and 2). In these equations, V, m, ρ are the volume, mass, and density of Au or polydopamine (PDA), as indicated by the subscripts. The mass ratio between PDA and pure Au in the superparticles can be obtained from the TGA data. The volume of

Au solid/element in the superstructure is calculated as 32.3% (equation 1) and the effective density of the superparticles is 7.09 g/cm^3. However, the volume of air in the superparticles (those occupied by the voids between the branches) was not taken into account. The calculated numbers may thereby deviate significantly from the real values.

$$\frac{V_{Au}}{V_{Au}+V_{PDA}} = \frac{\frac{m_{Au}}{\rho_{Au}}}{\frac{m_{Au}}{\rho_{Au}}+\frac{m_{PDA}}{\rho_{PDA}}} = \frac{\frac{1}{\rho_{Au}}}{\frac{1}{\rho_{Au}}+\frac{(m_{PDA}/m_{Au})}{\rho_{PDA}}} \quad (1)$$

$$\rho_{superparticle} = \frac{\rho_{Au}V_{Au}+\rho_{PDA}V_{PDA}}{V_{Au}+V_{PDA}} = \frac{V_{Au}}{V_{Au}+V_{PDA}} \times \left(\rho_{Au} + \rho_{PDA}\frac{V_{PDA}}{V_{Au}}\right) \quad (2)$$

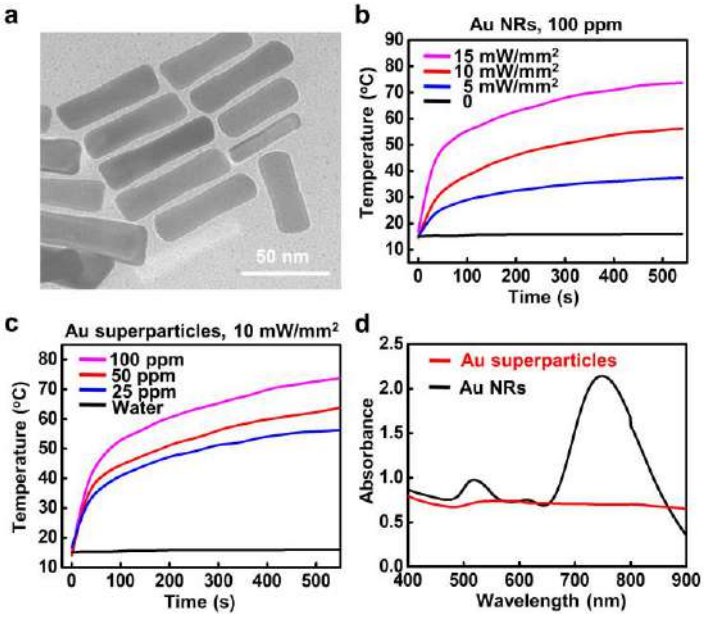

Figure S2. Additional data on photothermal properties of Au superparticles and Au NRs. (a) The TEM image of Au NRs. **(b)** Temporal temperature changes of a solution of Au NRs (100 ppm) under continuous 808 nm irradiation at different laser power densities (0, 5, 10, 15 mW/mm^2). **(c)** Temporal temperature changes of solutions of Au superparticles with different concentration (0, 25, 50, 100 ppm) when exposed to continuous 808 nm laser (10 mW/mm^2). **(d)** Comparison of the absorption spectra of solutions (100 ppm) of Au superparticals and Au NRs.

We tested the TGA of Au superparticles/PDA ligands and Au NRs/CTAB ligands. The content of ligands in the Au superparticles or NRs was about 12% and 23%, respectively. Accordingly, the 100 ppm Au superparticle solution contains 88 ppm of pure Au and the 100 ppm NR solution contains 77 ppm of pure Au. We can then compare the photothermal conversion efficiency of Au superparticles and NRs based on the mass concentration of Au elements in these structures. One can calculate the molar

concentration of Au atoms ([Au]), regardless of their presence as superparticles or NRs, by using the equation (3). In this formula, [Au nanomaterials] is the concentration of Au superparticles or Au NRs (unit, g/L; 100 ppm is close to 0.1 g/L) and M_{Au} is the molar mass of Au (197 g/mol). The molar concentration of Au atoms ([Au]) in Au superparticles and Au NRs (both 100 ppm) is 0.447 and 0.390 mmol/L, respectively.

$$[\mathrm{Au}] = ([Au\ nanomaterials] \times \frac{m_{Au}}{m_{Au}+m_{ligands}})/M_{Au} \quad (3)$$

The calculated concentration of Au elements in the solutions of Au superparticles and NRs, in combination with the data shown in Fig. 2a,d, suggests that the Au superparticles are more effective in converting light energy into heat, when they have similar concentration of Au elements with Au NRs.

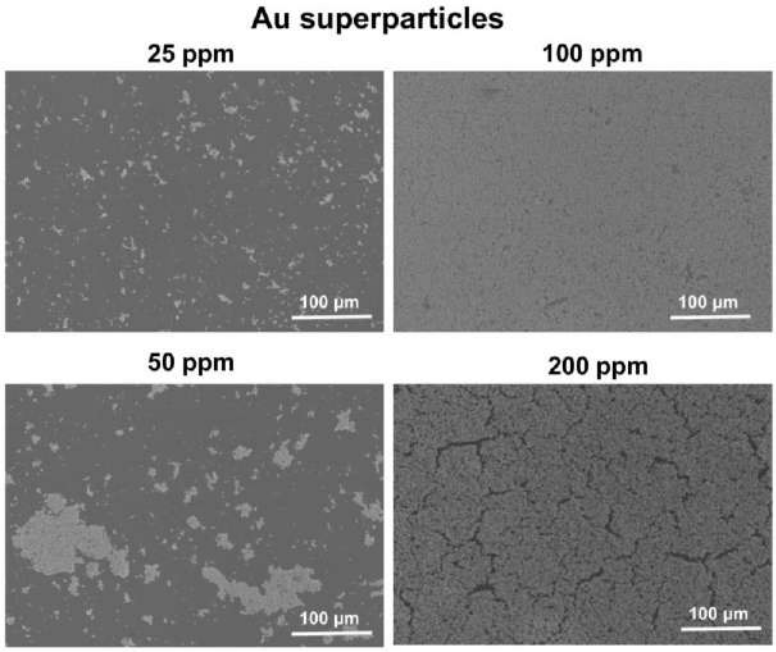

Figure S3. SEM images of films coated from Au superparticle solutions of different concentration.

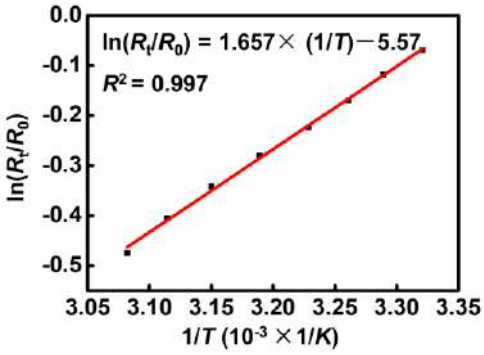

Figure S4. Calibration curve for the temperature measurements with patch clamp system. R_0 and R_t are the resistance of the micropipette at room temperature and temperature T. The black dots are measured data, which can be fit (the red trace) by the formula shown in the graph.

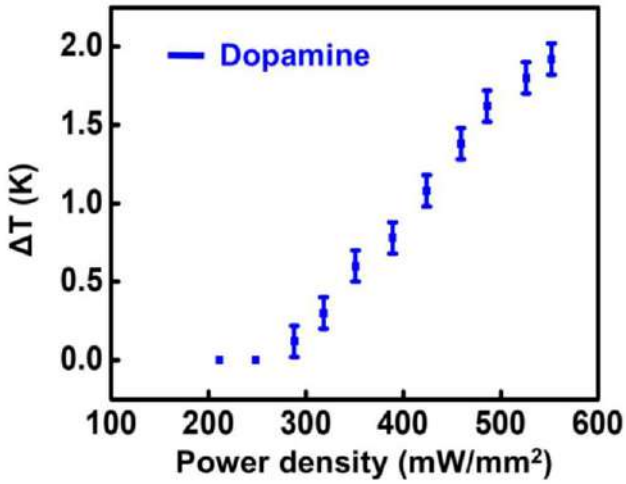

Figure S5. Temperature increases induced by dopamine films under irradiation. The dopamine films were coated from its solution (4 mg/mL). The irradiation used a 808-nm laser (1 ms, 1 Hz).

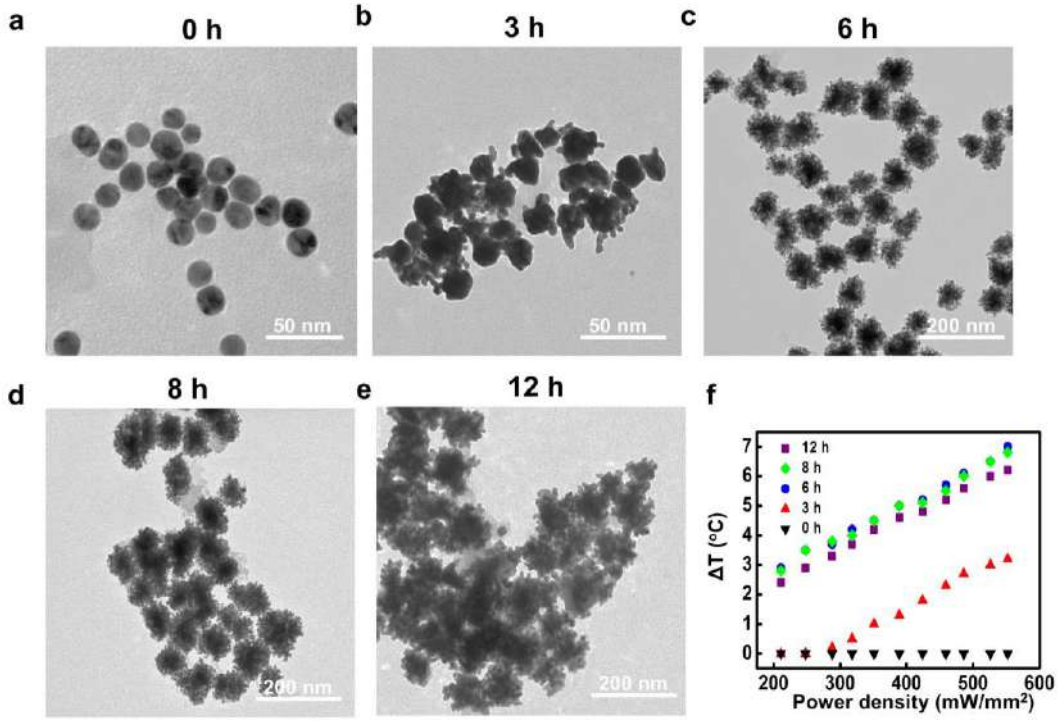

Figure S6. TEM images of Au superparticles synthesized with different reaction time and the temperature changes of Au superparticle films during irradiation. **(a−e)** TEM images. The temperature changes in panel **(f)** were recorded from films of these nanomaterials (coated from 100 ppm solutions) under the irradiation of 808 nm laser at various power densities with the duration of 1 ms.

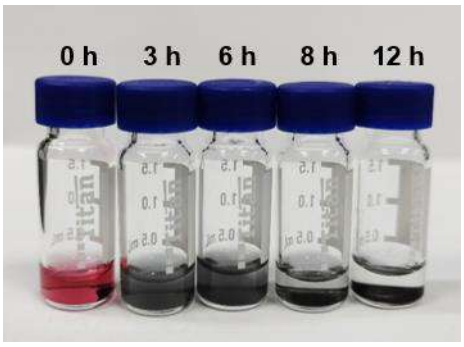

Figure S7. Photographs of solutions of Au nanostructures or superparticles synthesized with different reaction time and after stored undisturbed for 1 h. The concentration of Au seeds (the sample labeled as 0 h) and superparticles was 100 ppm and the solvent was ethanol.

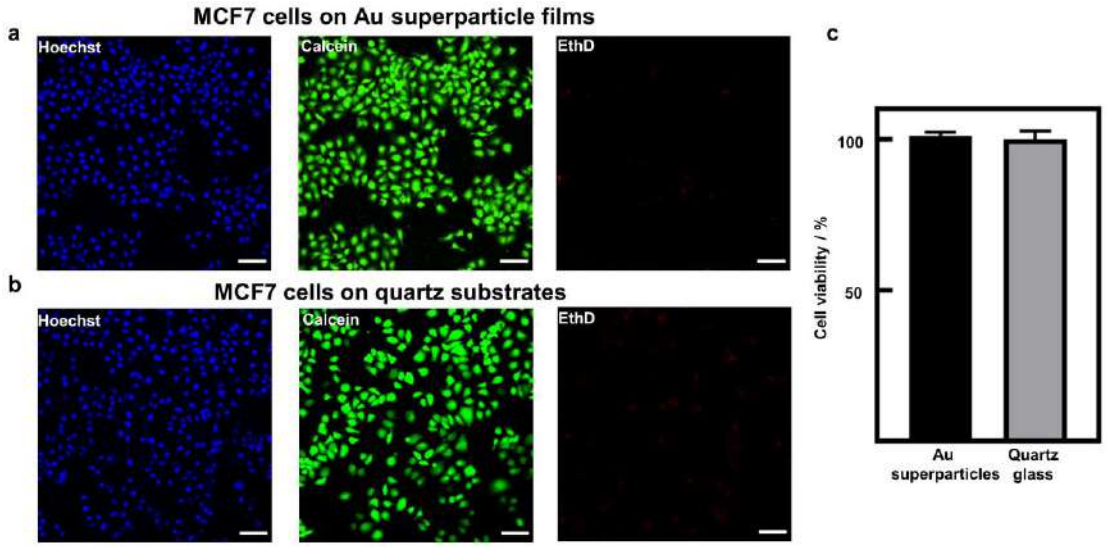

Figure S8. Cell biocompatibility of MCF7 cells cultured on Au superparticle films. **(a)** Live/dead assay of MCF7 cells incubated on Au superparticle films and **(b)** bare quartz substrates. The images with blue (Hoechst), green (Calcien AM), and red (Ethidium homodimer-1, EthD) colors represent cell nuclei, live cells, and dead cells, respectively. Scale bars are 100 μm. **(c)** Cell viability measured by CCK-8 assay of MCF7 cells incubated on Au superparticle films and on bare quartz substrates.

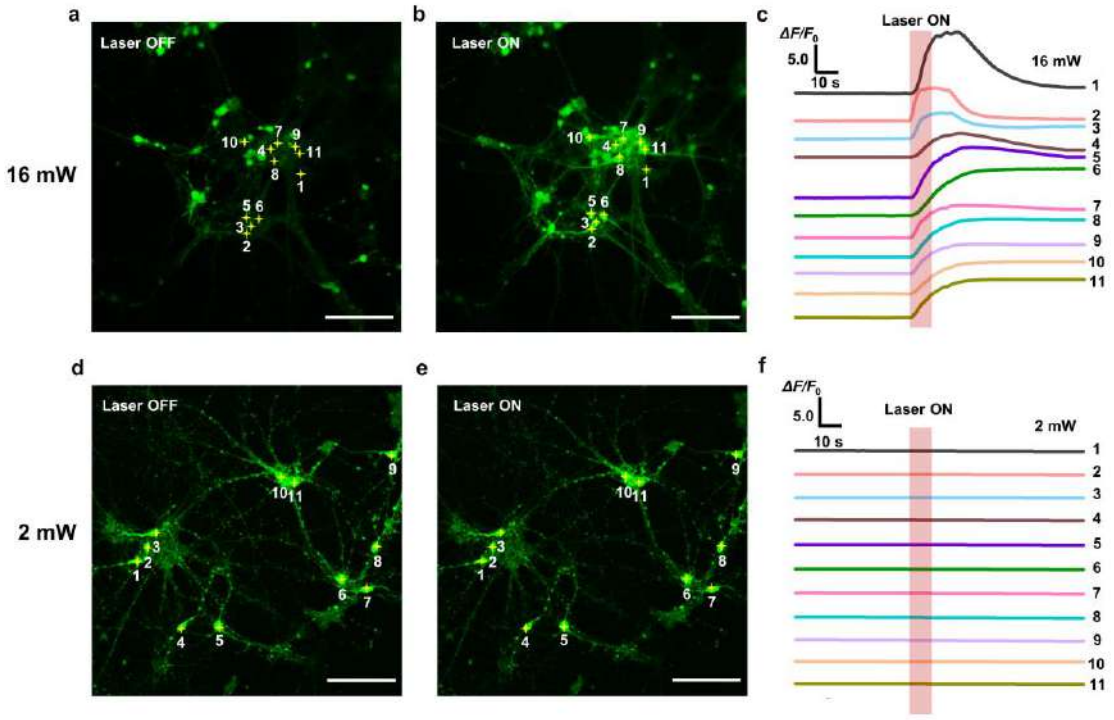

Figure S9. Photothermal stimulation of mouse hippocampal neurons cultured on Au superparticle films with different laser power. (a,b) Calcium imaging of stained mouse hippocampal neurons cultured on Au superparticle films taken when the 800 nm stimulation laser was off and on, respectively. The laser power was 16 mW. The neurons marked with yellow crosses were selected randomly as ROIs for fluorescence analysis. **(c)** Normalized $\Delta F/F_0$ over time of ROIs indicated in (a,b). The red bar denotes laser illumination time (10 s). **(d–f)** Corresponding data for neurons cultured on Au superparticle films taken when the laser power was 2 mW. Scale bars are 100 μm.

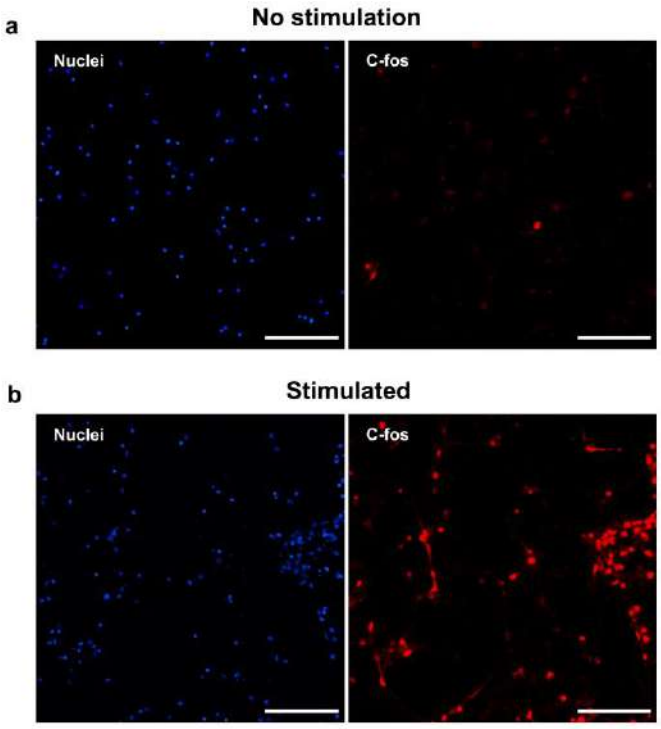

Figure S10. Fluorescent images of the expression of c-fos in mouse hippocampal neurons cultured on Au superparticle films before and after stimulation with 800 nm laser. The images with blue (DAPI) and red (Alexa Fluor 594) colors represent cell nuclei and c-fos, respectively. The mouse hippocampal neurons cultured on Au superparticle films were stimulated by the 800 nm laser (24 mW, 10 s). Scale bars are 100 μm.

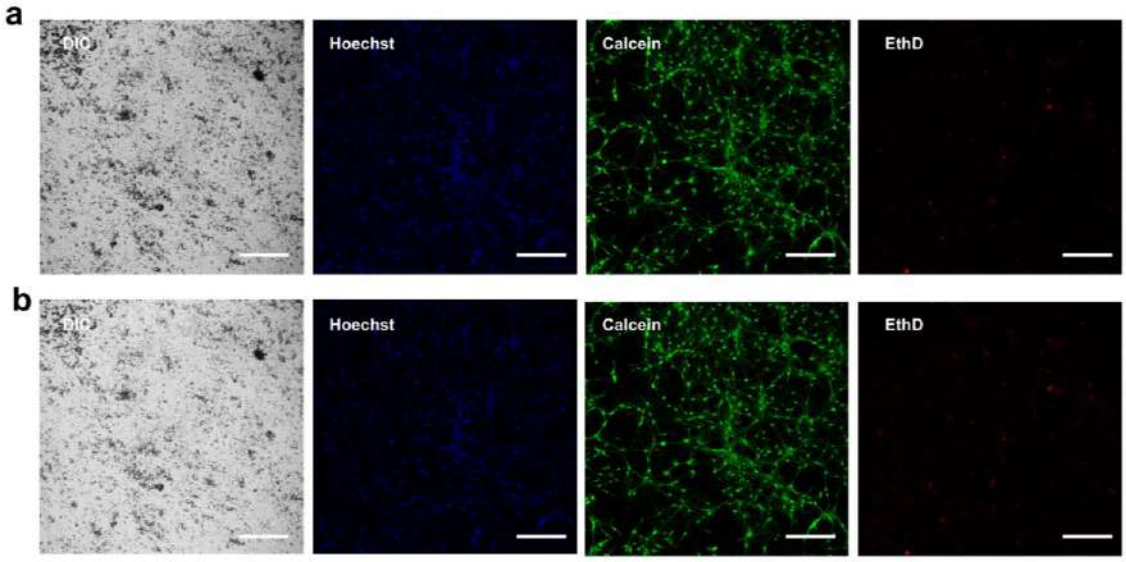

Figure S11. Cell viability of mouse hippocampal neurons cultured on Au superparticle films (a) before and (b) after photostimulation. The irradiation used a 808 nm laser with the intensity of 55.2 mW/mm^2 and duration of 10 s. The images with blue (Hoechst), green (Calcien AM), and red (EthD-1) color represent cell nuclei, live cells and dead cells, respectively. Scale bars are 100 μm.

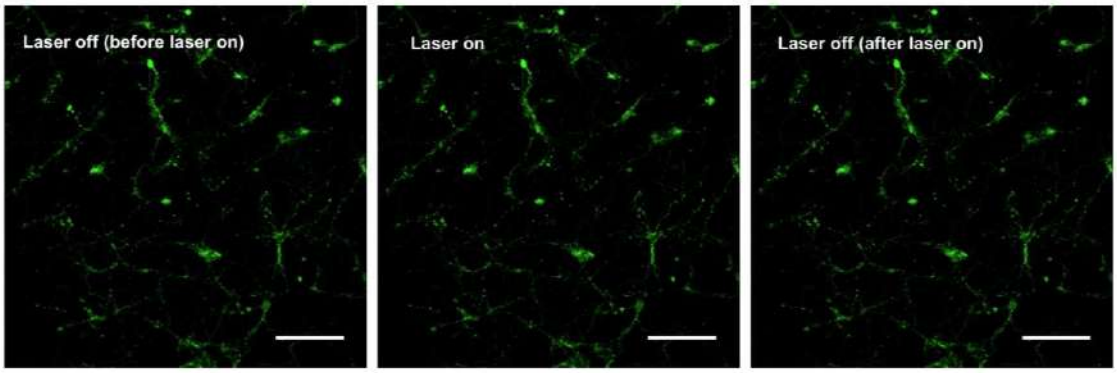

Figure S12. Calcium imaging of mouse hippocampal neurons cultured on polydopamine films under laser irradiation. Images from left to right correspond to the cases before laser was on (laser off), during laser irradiation (laser on), and after laser irradiation (laser off). A 808 nm laser (55.2 mW/mm^2, 10 s) was used for stimulation. Scale bars are 100 μm.

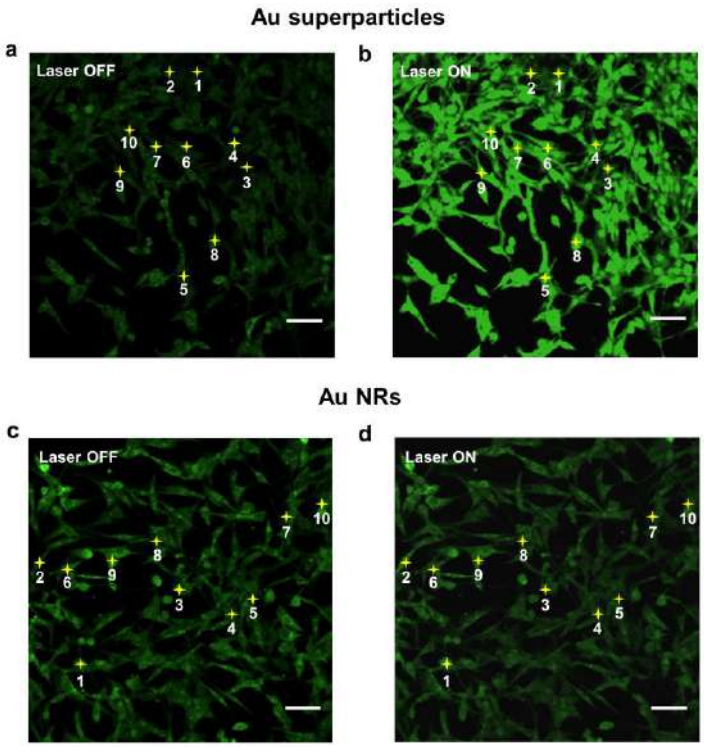

Figure S13. Comparison of films of Au superparticles and NRs in cell activity stimulation. (a,b) The calcium imaging of stained PC-12 cells (with the Ca^{2+} indicator, Calbryte 520 AM) cultured on Au superparticle films when the external 808 nm laser is (a) off and (b) on. The cells marked with yellow crosses indicate ROIs selected randomly for fluorescence analysis. **(c,d)** The calcium imaging of stained PC-12 cells (with the Ca^{2+} indicator, Calbryte 520 AM) cultured on Au NR films when the laser is (c) off and (d) on. The stimulation and imaging condition was identical for samples in (b,d) (55.2 mW/mm^2, 1 min). Scale bars are 100 μm.

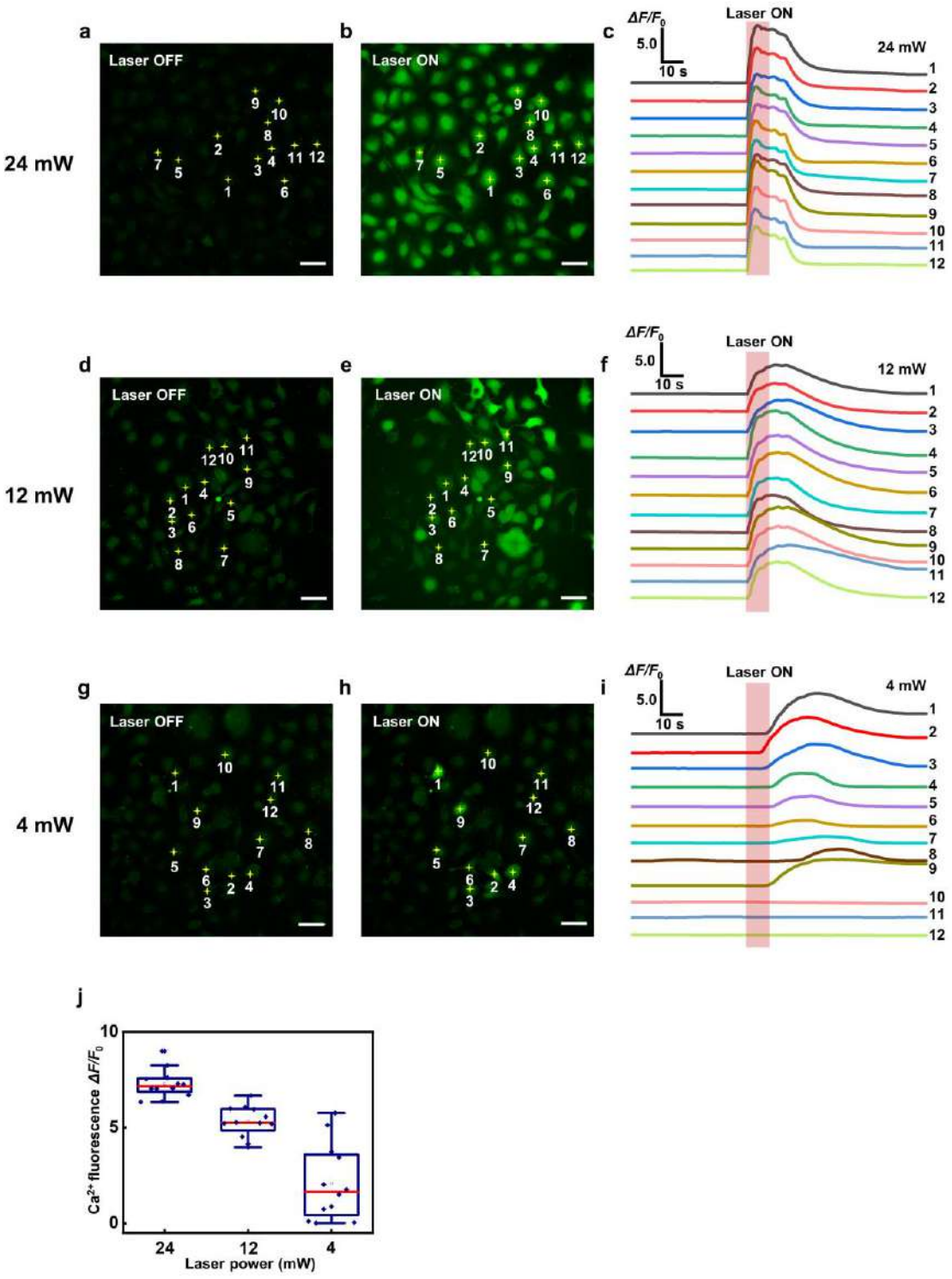

Figure S14. Photothermal modulation of MCF7 cell activities with different laser power. (a,b) The calcium imaging of MCF7 cells cultured on Au superparticle films when the 800 nm laser is (a) off and (b) on. The laser power was 24 mW. The cells marked with yellow crosses were selected randomly as ROIs for fluorescence analysis.

(c) Normalized $\Delta F/F_0$ of the ROIs (marked in a,b) as a function of time. The red bar denotes laser illumination time (10 s). **(d–f)** and **(g–i)** correspond to images and data collected under the laser power of 12 and 4 mW, respectively. **(j)** Normalized $\Delta F/F_0$ of MCF7 cells stimulated at different laser power. The statistics were based on data from all ROIs. Scale bars are 50 μm.

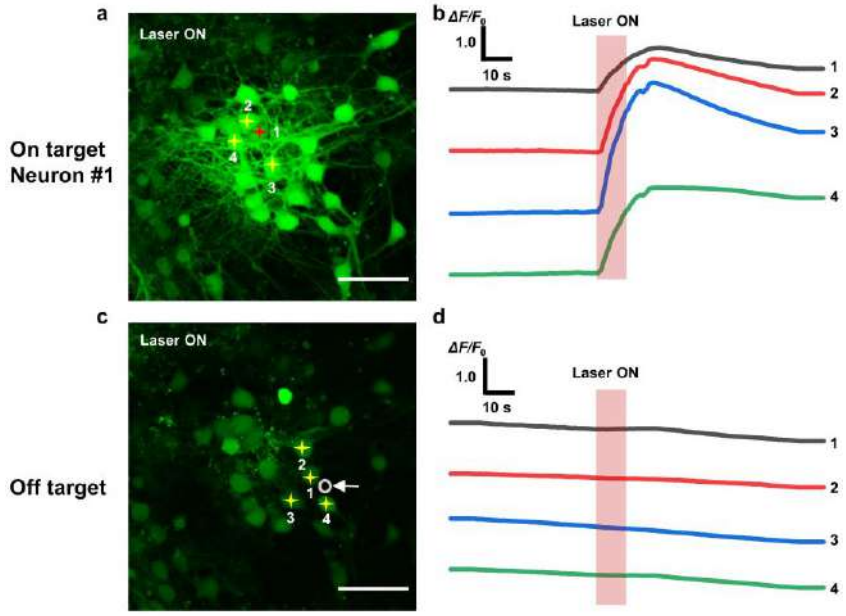

Figure S15. Additional data on the modulation of target neurons. (a,c) The calcium imaging of mouse hippocampal neurons cultured on Au superparticle films when the laser focuses (a) on target neuron #1 (marked by the red cross) or (c) in an off-cell area (indicated by the white circle). The laser was 800 nm with the power of 24 mW. **(b,d)** Normalized $\Delta F/F_0$ of neurons #1–#4, as marked with red and yellow crosses in (a,c). The red bar denotes laser illumination time (10 s). This comparison confirms the capability of precise stimulation of a single or a few cells. Panels (c,d) replicate those shown in Fig. 6 (a,d). Scale bars are 50 μm.

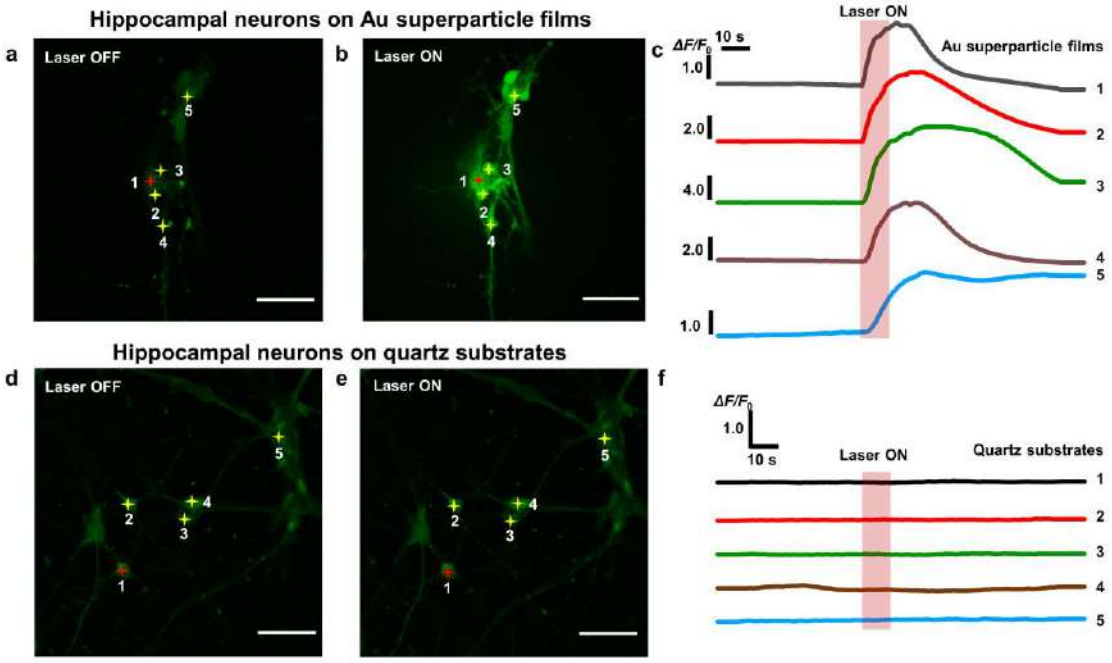

Figure S16. Modulation of target neurons cultured on Au superparticle films or quartz substrates. (a,b) Calcium imaging of mouse hippocampal neurons cultured on Au superparticle films when the laser is (a) off and (b) on. In (b), the laser was focused on the target neuron #1 (marked by red cross), which significantly increases the Ca^{2+} fluorescence of this neuron and its neighbors (#2–#5). The laser power was 8 mW. **(c)** Normalized $\Delta F/F_0$ over time of neurons marked in (b). The red bars denote laser illumination time (8 mW, 10 s). Beside the fluorescence of the ROI of target neuron (#1), ROIs of neurons (#2–#5) indicated by the yellow crosses are also used for fluorescence analysis. Panels **(d–f)** show data collected (24 mW, 10 s) but on neurons cultured on bare quartz substrate. No stimulation was observed. Scale bars are 50 μm.

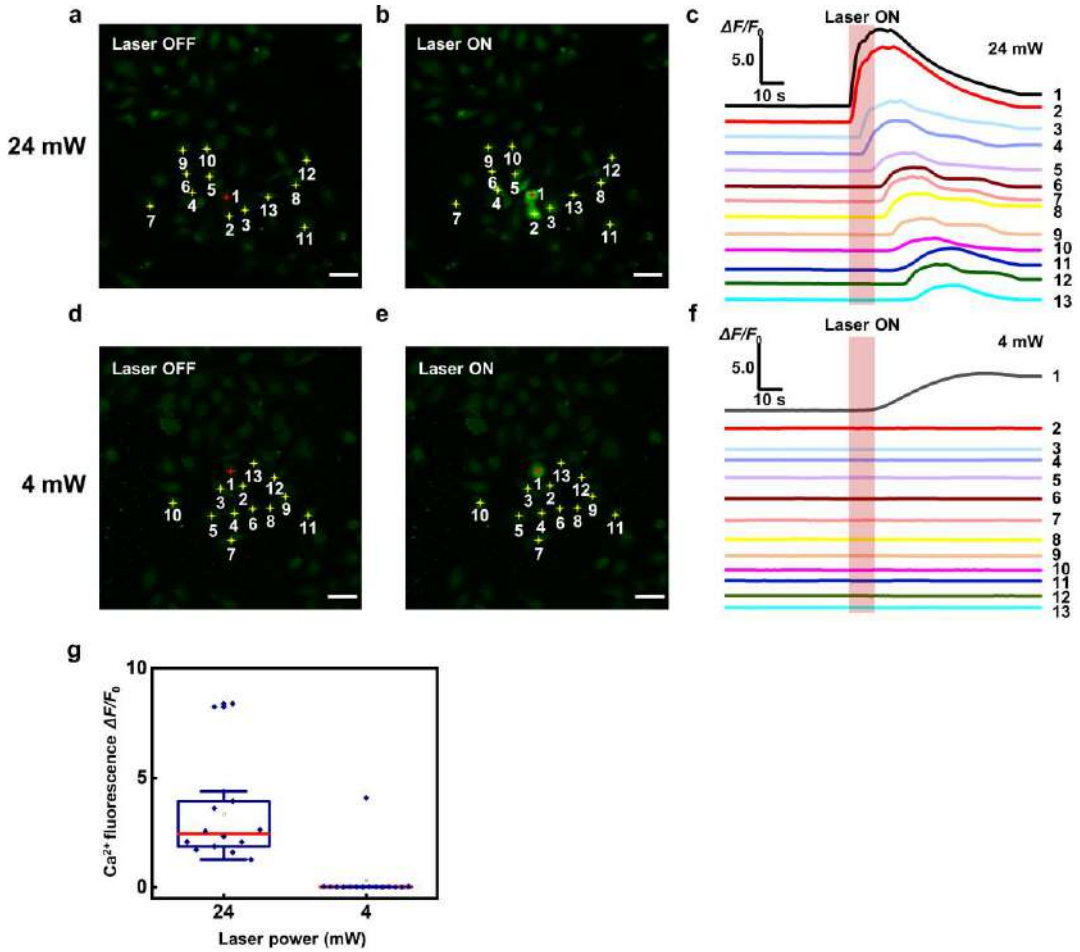

Figure S17. Modulation of target MCF7 cells cultured on Au superparticle films. **(a,b)** Calcium imaging of MCF7 cells cultured on Au superparticle films when the laser is (a) off and (b) on. In (b), the laser was focused on the target cell #1 (marked by the red cross). The laser power was 24 mW. **(c)** Normalized $\Delta F/F_0$ over time of cells marked in (a,b). The red bar denotes the laser illumination time (24 mW, 10 s). Beside the fluorescence of the ROI of target cell (#1), ROIs of other cells (indicated by the yellow crosses) are also used for fluorescence analysis. Panels **(d–f)** show data collected on cells cultured on Au superparticle films but at a lower laser power (4 mW, 10 s). **(g)** Comparison of normalized $\Delta F/F_0$ for cells irradiated by laser at different laser power. The statistics were based on data from all ROIs of the marked cells. Scale bars are 50 μm.

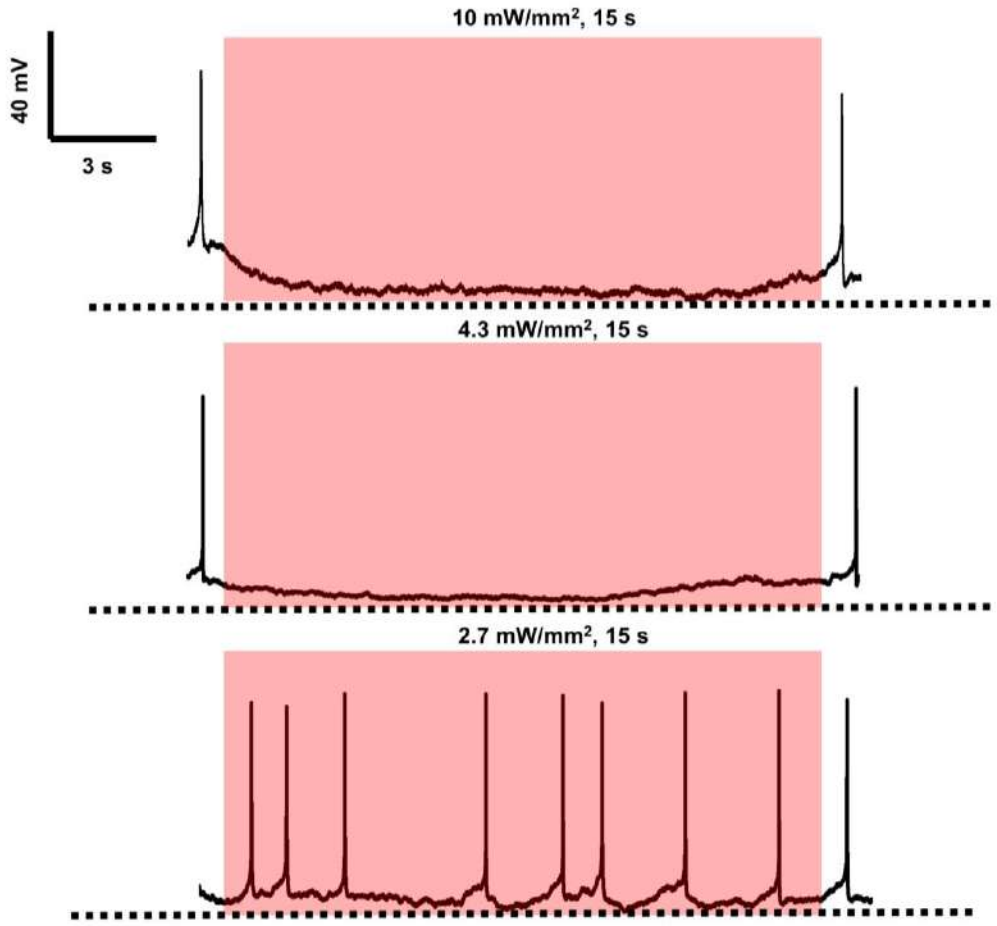

Figure S18. Membrane potential recordings of mouse hippocampal neurons cultured on Au superparticle films under 808 nm laser irradiation with various laser power density. The time scale was adjusted to show the delay in neuronal activity suppression after illumination (10 and 4.3 mmW/mm^2) and the delay in depolarization after ceasing the illumination. Illumination with low intensity (e.g., 2.7 mmW/mm^2) cannot inhibit neuronal activities.

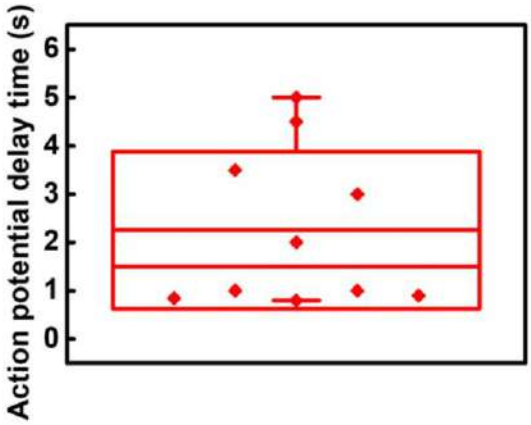

Figure S19. Statistics on the delay time of recurrence of the action potential in mouse hippocampal neurons after ceasing the laser illumination. Number of neurons = 10.

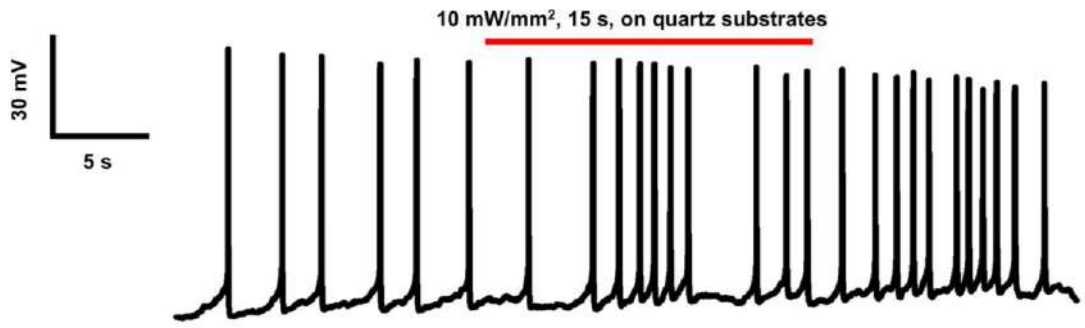

Figure S20. Action potential recordings of mouse hippocampal neurons cultured on bare quartz substrates. The mouse hippocampal neurons cultured on bare quartz substrates generated action potential firing after positive current injection. After 808 nm laser irradiation with the laser power density of 10 mW/mm^2 for 15 s, the neuronal action potential firing had no changes. Number of neurons = 3.

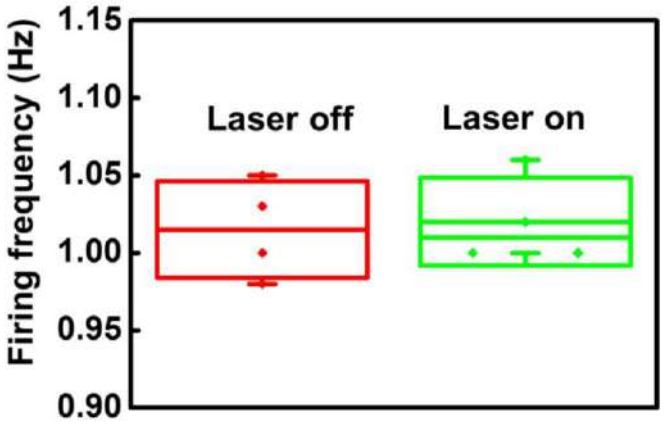

Figure S21. Statistics on frequency of firing of mouse hippocampal neurons cultured on bare quartz substrate before and after laser irradiation. Laser condition, 808 nm, 15 s, 10 mW/mm^2. Number of neurons = 3.

Table S1. Comparison of photothermal efficacy of various photothermal nanotransducers in solution states.

Materials	**Concentration (O.D.)**	**Laser wavelength (nm)**	**Light power density (mW/mm^2)**	**Approximate temperature change (K) (Irradiation duration)**	**Reference**
Au NRs	1	785	21	32	1
BSA-carbon nanohorns	0.7	785	15	27 (30 min)	2
Au nanostars	1	785	15	35 (4 min)	3
Polydopamine	0.7	808	14	16 (4 min)	4
Au NRs	0.7	808	10	40 (10 min) 33 (4 min)	This work
Au superparticles	0.7	808	10	52 (10 min) 42 (4 min)	This work

References

(1) Yoo, S.; Kim, R.; Park, J.-H.; Nam, Y. Electro-optical Neural Platform Integrated with Nanoplasmonic Inhibition Interface. *ACS Nano* **2016**, *10* (4), 4274-4281.

(2) Miyako, E.; Deguchi, T.; Nakajima, Y.; Yudasaka, M.; Hagihara, Y.; Horie, M.; Shichiri, M.; Higuchi, Y.; Yamashita, F.; Hashida, M.; et al. Photothermic regulation of gene expression triggered by laser-induced carbon nanohorns. *Proc. Natl. Acad. Sci. U.S.A.* **2012**, *109* (19), 7523-7528.

(3) Lee, J. W.; Jung, H.; Cho, H. H.; Lee, J. H.; Nam, Y. Gold nanostar-mediated neural activity control using plasmonic photothermal effects. *Biomaterials* **2018**, *153*, 59-69.

(4) Gholami Derami, H.; Gupta, P.; Weng, K.-C.; Seth, A.; Gupta, R.; Silva, J. R.; Raman, B.; Singamaneni, S. Reversible Photothermal Modulation of Electrical Activity of Excitable Cells using Polydopamine Nanoparticles. *Adv. Mater.* **2021**, *33* (32), 2008809.